Supporting Information

Visualizing the dynamic metalation state of New Delhi Metallo-β-lactamase-1 in bacteria using a reversible fluorescent probe

Radhika Mehta,[a] Dann D. Rivera,[b] David J. Reilley,[c] Dominique Tan,[a] Pei W. Thomas,[b] Abigail Hinojosa,[a] Alesha C. Stewart,[b] Zishuo Cheng,[d] Caitlyn A. Thomas,[d] Michael W. Crowder,[d] Anastassia N. Alexandrova,[c] Walter Fast,*[b] Emily L. Que*[a]

[a] Department of Chemistry, University of Texas at Austin, 105 E 24th St Stop A5300, Austin, TX 78712

[b] Division of Chemical Biology & Medicinal Chemistry, College of Pharmacy, University of Texas, Austin, Texas 78712

[c] Department of Chemistry and Biochemistry, University of California-Los Angeles, 607 Charles E. Young Drive, Los Angeles, California 90095-1569

[d]Department of Chemistry and Biochemistry, Miami University, Oxford, Ohio 45056

General Procedures

All synthesis reagents were purchased from TCI America, ACROS, Alfa Aesar or Sigma Aldrich. Bovine carbonic anhydrase II, myoglobin, BSA and alkaline phosphatase were purchased from Sigma Aldrich. NDM-1 and other metallo-β-lactamases were kindly provided by the Fast lab or the Crowder lab. Phosphotriesterase was kindly provided by Prof. Frank Raushel from Texas A&M University. For spectroscopic studies, 0.05 M HEPES, pH 7.0 containing 10 μM $ZnSO_4$ buffer was prepared and degassed. ^{1}H and ^{13}C NMR spectra were acquired on 400 MHz Agilent MR Spectrometers or Bruker AVIII HD 500. NMR samples were prepared in $(CD_3)_2CO$, $(CD_3)_2SO$, CD_3CN, or $CDCl_3$, and chemical shifts are reported in ppm. Spectroscopic studies were performed using Agilent Cary 60 UV-Vis spectrophotometer. Fluorescence spectroscopic measurements were made using an Agilent Cary Eclipse fluorescence spectrofluorometer. Confocal imaging was performed on Zeiss 710 Laser Scanning Confocal Microscope using a 40X lens. Live-cell imaging was performed using ibidi μ-slide 8-well glass bottom dishes or glass cover slips.

Synthetic Procedures

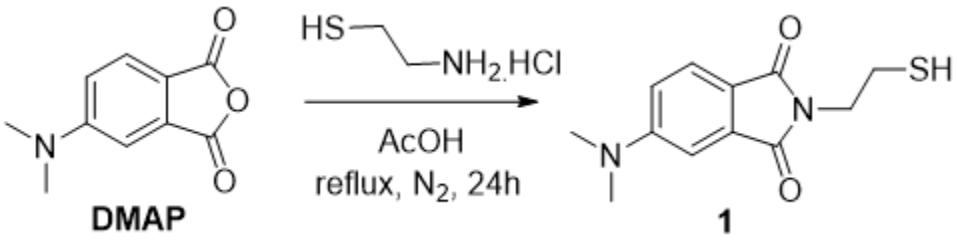

Scheme S1: Synthesis of **1**

*Synthesis of **1***: To a solution of DMAP (40 mg, 0.2 mmol) in acetic acid (5 mL), was added cysteamine (2.5 equiv). The reaction was refluxed for 24 hours and the formation of the product was monitored *via* TLC in 1:1 Dichloromethane (DCM) - hexane mixture. The solvent was then evaporated on a rotary evaporator, and the product was purified by silica gel chromatography

using 40%DCM/hexane to 60%DCM/hexane mixture. Yellow solid (90% yield). HRMS (ESI^+): m/z calcd 273.0668 ($M+Na^+$), found 273.0671. ^1H NMR (400 MHz, Chloroform-d_3) δ 7.64 (d, J = 8.5 Hz, 1H), 7.07 (d, J = 2.4 Hz, 1H), 6.79 (dd, J = 8.5, 2.4 Hz, 1H), 3.81 (dd, J = 7.9, 6.5 Hz, 2H), 3.11 (s, 5H), 2.85 – 2.74 (m, 2H), 1.42 (t, J = 8.6 Hz, 1H). ^{13}C NMR (101 MHz, CD_3CN) δ 169.66, 169.27, 155.67, 135.69, 125.31, 118.32, 115.75, 106.14, 41.32, 40.72, 23.51, 1.94, 1.73, 1.53, 1.32, 1.11, 0.91, 0.70.

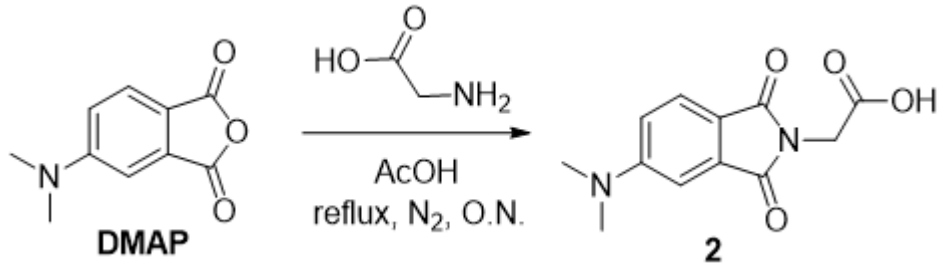

Scheme S2: Synthesis of **2**

*Synthesis of **2**:* To a solution of DMAP (50 mg, 0.26 mmol) in acetic acid (5 mL) was added glycine (2.5 equiv). The reaction was refluxed overnight, and the solvent was evaporated on a rotary evaporator. The product was purified by reverse phase chromatography using 50% MeOH-water with 0.1% formic acid. Yellow solid (40% yield). HRMS (ESI^+): m/z calcd 249.0870 ($M+H^+$), found 249.0873. ^1H NMR (400 MHz, Acetone-d_6) δ 7.60 (dd, *J* = 8.5, 0.4 Hz, 1H), 7.05 (d, *J* = 2.4 Hz, 1H), 6.95 (dd, *J* = 8.5, 2.5 Hz, 1H), 4.29 (s, 2H), 3.13 (s, 6H). ^{13}C NMR (Acetone-d_6) δ 205.31, 167.81, 167.27, 154.72, 134.74, 124.47, 117.27, 114.95, 105.25, 39.61, 38.20, 29.68.

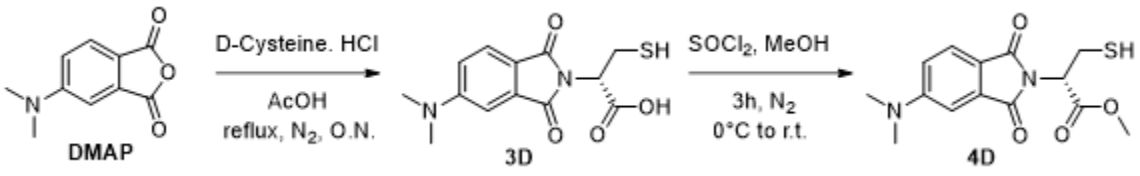

Scheme S3: Synthesis of probes **3D** and **4D**

*Synthesis of **3D**:* To a solution of DMAP (70 mg, 0.36 mmol) in acetic acid (4 mL), was added D-cysteine•HCl (3 equiv). The reaction was refluxed overnight, and the formation of the product was monitored *via* TLC using 1:1 DCM-hexanes mixture. To avoid disulfide formation, the solution was kept under nitrogen at all times. If formation of disulfide was observed *via* LCMS (mass: 586), then 2 equiv. of TCEP in methanol/water (2:1) was added, and the reaction stirred overnight. The solvent was then evaporated on a rotary evaporator, and the product was purified using reverse phase chromatography using 30% acetonitrile-water mixture (with 0.1% formic acid). Yellow solid (55% yield). HRMS (ESI^+): m/z calcd 317.0566 ($M+Na^+$), found 317.0568. ^1H NMR (400 MHz, Acetone-d_6) δ 7.64 (d, J = 8.5 Hz, 1H), 7.08 (d, J = 2.4 Hz, 1H), 6.99 (dd, J = 8.5, 2.1 Hz, 1H), 4.88 (dd, J = 10.4, 5.2 Hz, 1H), 3.34 (d, J = 20.7 Hz, 2H), 3.17 (s, 6H). ^{13}C NMR (101 MHz, acetone) δ 205.26, 205.25, 205.24, 205.23, 205.22, 167.91, 167.37, 154.84, 134.43, 124.61, 116.90, 115.14, 105.31, 54.23, 39.62, 23.33.

*Synthesis of **4D***: To a solution of **3D** (0.1 mmol) in anhydrous methanol (2 mL) at 0°C was added thionyl chloride dropwise (0.1 mL). The reaction was allowed to reach room temperature and run for 3 hours to allow formation of the product. The solvent was then removed under vacuum. If formation of disulfide was observed *via* LCMS, then 2 equiv. of TCEP in methanol/water (2:1) was added and the reaction was stirred overnight. The solvent was then evaporated on a rotary evaporator, and the product was purified using reverse phase chromatography using 40% acetonitrile-water mixture (with 0.1% formic acid). Yellow solid (68% yield). HRMS (ESI^+): m/z calcd 331.0723 ($M+Na^+$), found 331.0724. ^1H NMR (Acetone-d_6, δ): 7.63 (dd, J = 8.6, 0.5 Hz, 1H), 7.07 (d, J = 2.4 Hz, 1H), 7.00 (dd, J = 8.6, 2.4 Hz, 1H), 4.89 (dd, J = 10.4, 5.1 Hz, 1H), 3.68 (s, 3H), 3.41 – 3.21 (m, 2H), 3.15 (d, J = 1.8 Hz, 6H), 1.97 (dd, J = 9.4, 8.2 Hz, 1H). ^{13}C NMR (Acetone-d_6) δ 205.20, 168.63, 167.78, 167.21, 154.85, 134.33, 124.67, 116.73, 115.17, 105.35, 54.17, 52.05, 39.62, 29.36, 29.17, 28.97, 28.78, 23.34.

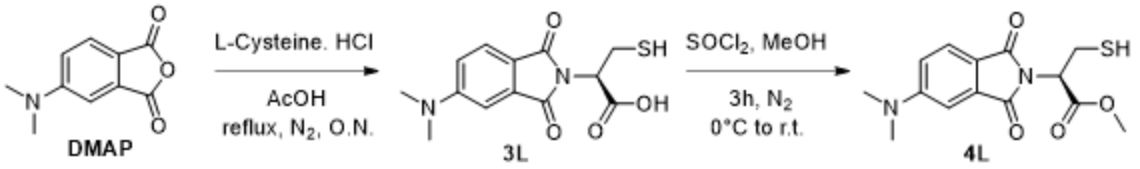

Scheme S4: Synthesis of probes **3L** and **4L**

*Synthesis of **3L***: To a solution of DMAP (70 mg, 0.36 mmol) in acetic acid (4 mL) was added L-cysteine•HCl (1.1 equiv). The reaction was refluxed overnight, and the formation of the product was monitored *via* TLC using 1:1 DCM-hexanes mixture. The solvent was then evaporated on a rotary evaporator, and the product was purified using reverse phase chromatography using 30% acetonitrile-water mixture (with 0.1% formic acid). Yellow solid (25% yield). HRMS (ESI^+): m/z calcd 317.0566 ($M+Na^+$), found 317.0567. ^1H NMR (400 MHz, Acetonitrile-d_3) δ 7.64 (d, J = 8.6 Hz, 3H), 7.09 (d, J = 2.4 Hz, 3H), 6.93 (dd, J = 8.6, 2.5 Hz, 3H), 4.76 (dd, 1H), 3.28 (d, J = 14.1 Hz, 2H), 3.1 (s, 6H).

*Synthesis of **4L***: To a solution of **3L** (15 mg, 0.05 mmol) in anhydrous methanol (2 mL) at 0°C was added thionyl chloride dropwise (0.1 mL). The reaction was allowed to reach room temperature and run for 3 hours to allow formation of the product. If formation of disulfide was observed *via* LCMS, then 2 equiv. of TCEP in methanol/water (2:1) was added, and the reaction was stirred overnight. The solvent was then evaporated on a rotary evaporator, and the product was purified using reverse phase chromatography using 40% acetonitrile-water mixture (with 0.1% formic acid). Yellow solid (50% yield). HRMS (ESI^+): m/z calcd 331.0723 ($M+Na^+$), found 331.0729. ^1H NMR (CD_3CN, δ): 7.64 (d, J = 8.6 Hz, 1H), 7.09 (d, J = 2.5 Hz, 1H), 6.94 (dd, J = 8.6, 2.5 Hz, 1H), 4.84 (dd, J = 10.4, 5.1 Hz, 1H), 3.67 (s, 3H), 3.13- 3.4 (m, 2H), 3.1 (s, 6H), 1.80 (t, J = 8.8 Hz, 1H).

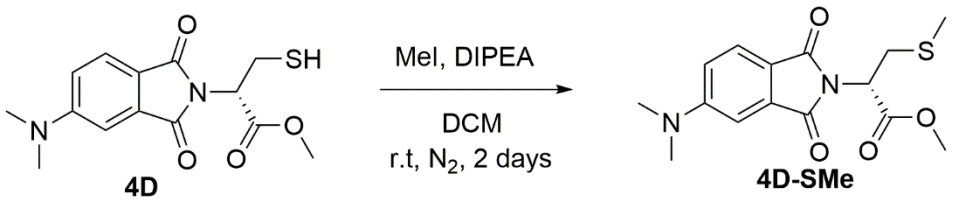

Scheme S5: Synthesis of probe **4D-SMe**

*Synthesis of **4D-SMe***: To a solution of **4D** (10.6 mg, 0.034 mmol) in anhydrous DCM (3 mL) at room temperature was added methyl iodide (2 equiv) and DIPEA (2 equiv.). The reaction was run overnight and an additional 2 equivalents of methyl iodide was added to allow formation of the product over the weekend until none of **4D** was detected via TLC and LCMS. The solvent was then evaporated on a rotary evaporator, and the crude mixture was purified using reverse phase chromatography using 45% acetonitrile-water mixture (with 0.1% formic acid). Yellow solid (63% yield). HRMS (ESI^+): m/z calcd 345.0879 ($M+Na^+$), found 345.0888. ^1H NMR (400 MHz, cd_3cn) δ 7.64 (dd, *J* = 8.5, 0.5 Hz, 1H), 7.10 (dd, *J* = 2.5, 0.4 Hz, 1H), 6.94 (dd, *J* = 8.6, 2.5 Hz, 1H), 5.02 – 4.93 (m, 1H), 3.69 (d, *J* = 0.3 Hz, 3H), 3.30 – 3.19 (m, 2H), 3.11 (s, 6H), 2.06 (s, 3H).

Characterization

Spectroscopic studies

Spectroscopic studies were performed using 2 mM stock solutions of the probes in acetonitrile (kept on ice at all times and made fresh every day to avoid disulfide formation). Quantum yields (Φ) for the probes in methanol were measured using quinine sulfate in 0.1 M H_2SO_4 (Φ = 0.54) as standard similar to Mehta *et. al*.[1]

Probe titrations with NDM-1

Binding studies were performed using purified New Delhi Metallo-β-lactamase-1 proteins with the first 35 amino acids truncated to produce a soluble protein (Δ35-NDM-1, see below) in degassed

50 mM HEPES, pH 7.0, containing 10 μM $ZnSO_4$. The probe concentration (**1-4L**) was kept at 10 μM with up to 3 equivalents of NDM. All studies were conducted at room temperature with λ_{ex} = 420 nm and λ_{em}= 430-800 nm. The fluorescence fold turn-on was plotted as a ratio of the fluorescence intensity integrated from 435-800 nm for the probe-protein vs the probe only.

Substrate (chromacef) assay

The enzymatic activity of Δ35-NDM-1 was monitored using chromacef as the substrate.[2] The formation of the hydrolyzed product was followed spectroscopically at 442 nm over 30 seconds in degassed 50 mM HEPES, pH 7.0, containing 10 μM $ZnSO_4$. In this assay, the enzyme and chromacef concentrations were kept constant at 20 nM and 20 μM, respectively, while the probe concentration was varied between 5- 150 μM (with 150 μM TCEP to avoid disulfide formation). The IC_{50} was determined by plotting fractional activity versus probe concentration (Activity = 1.0 when no probe is added), with each value determined in triplicate. The resulting points were fit using a one phase exponential decay on GraphPad Prism to determine IC_{50}, with fitting errors reported.

Preparation of Co(II)-substituted NDM-1 for UV-visible spectroscopy

Co(II)-substituted NDM-1 was prepared by dialyzing purified NDM-1 against each of the following 500 mL buffers for 12 h at 4 ℃: 50 mM HEPES, pH 6.8 containing 500 mM NaCl, 2 mM EDTA twice; and 50 mM HEPES, pH 6.8 containing 500 mM NaCl, 0.5 g Chelex three times. A stock solution was prepared containing the following: 300 μM NDM-1 in 50 mM HEPES, pH 6.8, containing 500 mM NaCl, 2 mM TCEP, and 10% glycerol. The NDM-1 stock solution and acetonitrile (solvent used to dissolve **4D**) were degassed using argon for 10 min prior to analysis. Two molar equivalents of $CoCl_2$ (from 100 mM stock solution made from Sigma-Aldrich; cat number 409332) were added to 500 μL of the protein stock. The sample was incubated for 30 sec, then 1 equivalent of compound **4D** was added. The sample was incubated 30 sec and then

centrifuged for 1 min. The mixture was added to a 500 μL quartz cuvette, and UV-vis spectra were obtained on a PerkinElmer Lambda 750 UV/vis/NIR spectrometer measuring absorbance between 300 and 700 nm at 25°C. A blank spectrum of 300 μM metal-free NDM-1 in 50 mM HEPES, pH 6.8, containing 500 mM NaCl, 2 mM TCEP, and 10% glycerol was used to generate difference spectra. All data were normalized to the absorbance at 800 nm.

Treatments with zinc chelators and inhibitors in vitro

For treatments with TPEN, DL-captopril and dipicolinic acid (DPA), stock solutions were prepared either in acetonitrile or DMSO (5- 25 μM). To a mixture of Δ35-NDM-1 and probe **4D** (3:1, 10 μM probe, 50 mM HEPES, pH 7.0 containing 10 μM $ZnSO_4$) was added each of the chelator/inhibitor in increasing equivalents, and the fluorescence spectra recorded.

We also conducted experiments with 15 min pre-incubation of NDM-1 (10 μM, 50 μM) with TPEN (50 μM) followed by **4D** addition (10 μM). This was done in 50 mM HEPES pH 7.0 and finally up to 50 μM $ZnSO_4$ was added to track fluorescence recovery.

For PAR treatment, 50 μM PAR was pre-mixed with Δ35-NDM-1 (10 μM) for 15 mins and then fluorescence spectra were recorded after addition of probe **4D**. We also recorded the NDM-1- **4D** fluorescence in the presence of PAR-Zn complex to ascertain any effects of the complex on overall fluorescence.

All studies were recorded at room temperature with λ_{ex}= 420 nm and λ_{em}= 430-800 nm.

Selectivity studies

Selectivity was tested by monitoring the fluorescence turn-on for probe **4D** (10 μM) at 1-3 equivalents of each protein. The fluorescence turn-on was monitored with bovine CAII, human CAII, myoglobin (Mb), Cu,Zn-SOD, Bovine serum albumin (BSA), alkaline phosphatase (AKP)

and phosphotriesterase (PTE). All studies were recorded at room temperature with λ_{ex}= 420 nm and λ_{em}= 430-800 nm.

Selectivity with other metallo-β-lactamases (MBLs) was tested by monitoring the fluorescence turn-on for probe **4D** (10 μM) at 1-3 equivalents of each MBL in degassed 50 mM HEPES, pH 7.0 containing 10 μM $ZnSO_4$. The solution was then treated with additional $ZnSO_4$, and the integrated fluorescence response was recorded at a final concentration of 50 μM $ZnSO_4$. All studies were conducted at room temperature with λ_{ex}= 420 nm and λ_{em}= 430-800 nm.

Native SDS PAGE

Native SDS PAGE was performed similar to previously-reported literature[1, 3] with 0.01% SDS. Protein-probe (**4D**) samples were prepared and incubated with excess TCEP (10 mins), then sample buffer (100 mM Tris HCl, 150 mM Tris Base, 0.01875% bromophenol blue, 1% SDS and 20% glycerol) was added before loading onto precast 4-20% Mini-Protean TGX (Biorad). Tris-MOPS running buffer, pH 7.7, was prepared and chilled at 4°C prior to the run. Samples were loaded into the gel, and electrophoresis was conducted at 120 V at 4°C for 40 mins. Fluorescence was recorded under UV light (short wave, 254 nm) to excite the NDM-bound fluorophore. The gels were then incubated with Coomassie overnight to visualize all the proteins bands.

Cellular studies

Escherichia coli BL21 (DE3) with the various NDM-1 expression constructs (pET27b-NDM1-WT (vector pET27b-NDM1-6H from Thomas et al.[4])), pET27b-NDM1-C26A (see below), pET27b-NDM1-Δ35 (vector pET27b-Strep-NDM1 from Thomas *et. al*,[4] pET27b-NDM15-Δ35 (see below)) were grown in LB broth supplemented with kanamycin (50 μg/mL) overnight at 37°C. An aliquot of this culture was then used to inoculate a fresh culture (1:100 dilution). When the culture grew to an OD of 0.5, it was supplemented with 50 μM $ZnSO_4$, and protein production was induced with

0.5 mM IPTG for all pET vectors. After 1 h, cells were harvested (or stored for a few hours prior at 4°C) for cell lysis or imaging experiments. The pHSG298 vector from Stewart et al.[5] was grown in *Escherichia coli* DH5α cells. For the pHSG298 vector, cells were grown for 5.5 h and then harvested for cell imaging.

Construction of pET27b-NDM15-Δ35 and pET27b-NDM1-C26A

To incorporate the coding sequence for NDM-15 into a vector parallel to pET27b-NDM1-Δ35, we replaced the NDM-1 coding sequence with that of NDM-15. Briefly, these expression vectors remove the coding sequence for the first 35 amino acids of the protein to generate soluble variants, add sequence encoding an N-terminal strep II tag followed by a tobacco etch virus (TEV) protease cleavage site, and provide a 5' *NcoI* restriction site and 3' *BamHI* restriction site. This insert was ligated into an appropriately digested pET27b expression vector behind the sequence encoding a PelB leader sequence to translocate expressed soluble Strep-Δ35-NDM15 to the periplasm. To generate this insert, the template (pET15b-His6-TEV-NDM-15 from Cheng *et. al*[6]) was used along with the forward primer 5′-tggCCATGG*attggagccacccgcaatttgaaaaggaaaacctgtatttccaa*ggccagcaaatggaaactggc-3′ (NcoI site capitalized, sequence coding the Strep II tag and TEV cleavage site italicized), and reverse primer 5′-ttcGGATCCtcagcgcagcttgtcggccat (*Bam*HI site capitalized). The PCR was conducted at 95° C for 4 min followed by 30 cycles of denaturation at 95° C for 30 s, annealing at 63° C for 30 s, and extension at 72° C for 60 s. The product was purified using a Qiagen PCR Purification kit (Qiagen, Valencia, CA), and digested with *Nco*I and *Bam*HI for 1 h at 37 °C. The pET27b-NDM1-Δ35 construct was digested with *Bam*HI and *Nco*I for 1 h at 37° C, and the digested pET27b expression vector scaffold was purified via gel excision using a Qiagen Gel Extraction kit (Qiagen, Valencia, CA). The digested and purified PCR product and pET27b vector scaffold were ligated using T4 DNA Ligase (NEB) for 30 min at 25 °C to form pET27b-NDM15-Δ35. The ligation product was used to transform TOP10 (ThermoFischer) cells via electroporation, and the

transformants grown with selection on LB agar plates with 50 μg/mL kanamycin. Plasmid DNA was purified from a culture grown from a single colony by using the Qiagen Miniprep kit (Qiagen, Valencia, CA), and the correct coding sequence was verified by DNA sequencing.

To create an expression vector that parallels pET27b-NDM1-WT (vector pET27b-NDM1-6H from Thomas *et. al*[4]) we used quick-change mutagenesis to change the codon for Cys26 (TGC) to instead code for Ala (GCT), resulting in the vector pET27b-NDM1-C26A. The coding sequence was verified by DNA sequencing a plasmid isolated from a culture grown from a single colony found on the initial selection plates, as above.

Cell lysis

For characterization of purified protein, following growth and induction, *E. coli* cells were recovered by centrifugation (5000 xg, 15 min, 4 °C) and lysed according to the ThermoScientific B-PER (bacterial protein extraction reagent #78248) protocol (ThermoScientific, Rockford, IL). The lysed cell fractions were then incubated with probe **4D**, TCEP, and sample buffer for 15 min before running the Native SDS PAGE.

Cell imaging experiments with various constructs

For imaging, the bacterial cell suspension in LB (OD 1- 1.5) was centrifuged at 3000 xg, 4 °C for 15 min and resuspended in M9 minimal medium. Prior to imaging, the cells were kept on ice during transport. For imaging, a 12 μM/15 μM stock solution of probe **4D** was prepared in M9 medium and added to the cell suspension to achieve a final OD of ~0.3-0.4 and probe concentration of 8/10 μM (total volume 100-300 μL). After 20 mins of incubation, the probe-cell suspension (10 μL) was added to a glass coverslip (24x50) #1 and covered with another smaller coverslip (9x9) just before imaging. It is essential to ensure no bubble formation or long wait times with the sample on the coverslip to minimize probe aggregation. Imaging was performed on the

Zeiss 710 Laser Scanning Microscope with the 40x lens at room temperature using λ_{ex}= 405 nm and λ_{em}= 486-614 nm.

Treatments to live cell imaging of NDM-1 and NDM-15

For treatment studies, Δ35NDM-1 (or Δ35NDM-15) was expressed for 1 h in *E. coli* BL21 (DE3) cells. The cells were centrifuged and resuspended in M9 media to achieve a final OD of ~0.3-0.4. Post-treatment with 8 μM probe **4D** (5 min), cells were subjected to the treatment of substrate (cephalexin), inhibitor (DL-captopril) or chelators.

Substrate: Cephalexin stock solution in DMSO (100 mM) was added to the probe-cell mixture to achieve a final substrate concentration of 1 mM. This cell mixture was then quickly imaged (2-3 mins preparation) over 10 min, recording images every 2-3 mins. The intensity density (representing fluorescence) was normalized to that of a parallel sample without cephalexin treatment (DMSO control) and the relative intensity densities plotted for each time point as described under image processing below.

Inhibitors/Chelators: The stock solution for each inhibitor/chelator was prepared in milliQ water, DMSO or acetonitrile (5-50 mM) for the different concentrations used. For calcium EDTA (CaEDTA) and N,N,N′,N′-*tetrakis*(2-pyridinylmethyl)-1,2-ethanediamine (TPEN), the stock solutions were prepared in MilliQ water, and DMSO, respectively (5 mM, 10 mM). For DL-captopril and dipicolinic acid (DPA), stock solutions of 50 mM each were prepared in acetonitrile and DMSO, respectively. The overall organic solvent concentration was kept below 1% *v*/*v* for each treatment. The **4D** treated cell mixture (5 min) was divided and incubated with different concentrations of each inhibitor/chelator to obtain the final desired concentrations ranging from 10-200 μM. These mixtures were incubated for 15 min and then imaged in triplicate at each concentration. These experiments were repeated 2-3 times over multiple days to ensure reproducibility. The images were processed and normalized against the 0 μM sample (organic

solvent control) for each set as detailed below. During acquisition of these images, the cell samples treated with the highest concentration of inhibitor/chelator were imaged first, and the 0 μM sample imaged last to minimize effects of time variation.

Image processing and quantification

Image processing of the fluorescence intensities was conducted using Fiji (or ImageJ), where the **4D** treated cells were represented in cyan or using the gems color scale (intensity 10-200).

The cells (fluorescent images only) were quantified individually by setting the threshold from 20-255 to measure the intensities. The intensities were analyzed for sizes 0.5-20 μm, circularity 0-1, and any dead (circular) or dividing (elongated) or overlapped cells were excluded from the data. Additionally, fluorescent dots due to probe aggregation, which appeared primarily in the high concentration treatment sets (like 200 μM DPA), were eliminated by comparing the fluorescence vs brightfield images for in-cell fluorescence. The intensity densities (representing fluorescence) for each treatment were normalized against the control (0 μM) for each set of treatment from an average of 3 images each collected over multiple days as shown in Figs. S12-15. These normalized intensities were averaged over all sets from 2-3 days, and two-way ANOVA analyses were performed to compare significance of the normalized intensity. The final average normalized intensity over multiple days from Figs. S12-15 were then plotted in Figs. 5 and 6.

Table S1. Spectroscopic properties of **1-4D** in methanol.

	1	**2**	**3D**	**3L**	**4D**	**4L**
Φ (MeOH)	0.008	0.021	0.028	0.027	0.007	0.012
ε ($M^{-1}cm^{-1}$)	4211	7100	3658	4652	5395	5035

The data was gathered and plotted as reported in Mehta *et. al.*[1] For quantum yield determination, quinine sulfate was used as a reference.

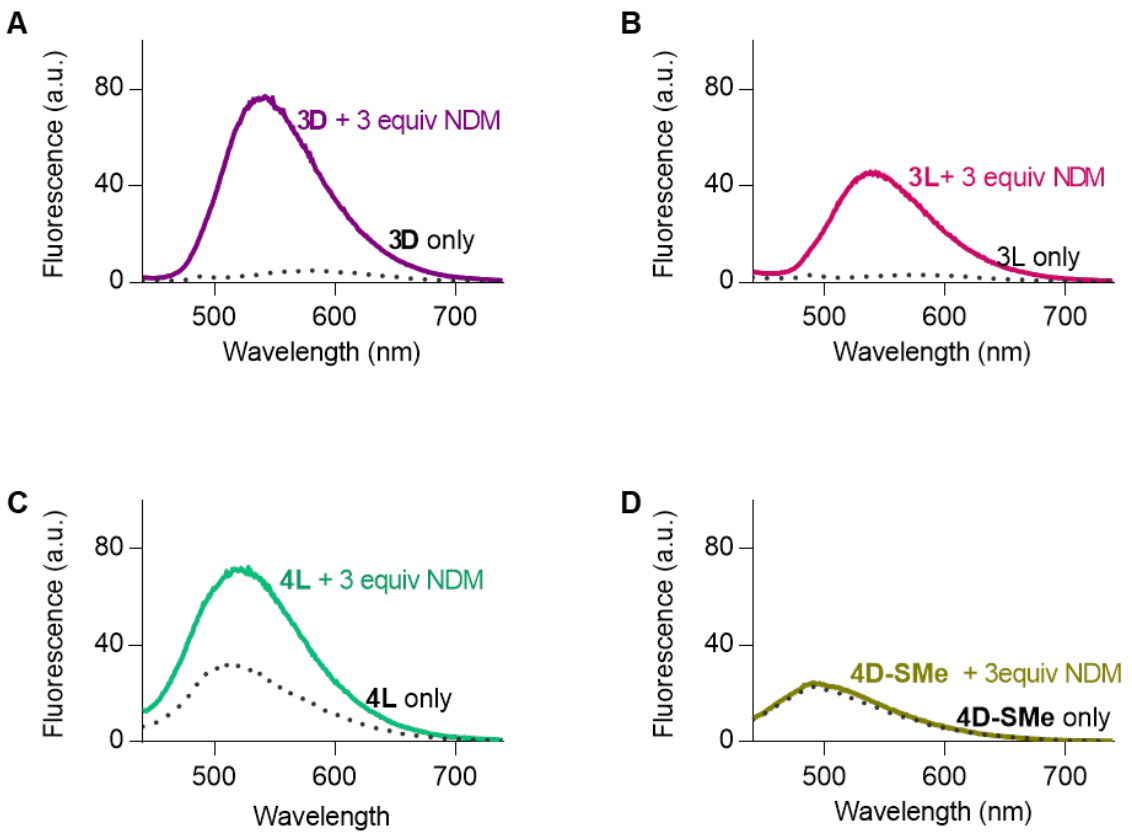

Fig. S1. Fluorescence turn-on graphs for probes **3D-4L** and **4D-SMe** with NDM-1 (3 equiv.) in 0.05 M HEPES, pH 7.0 containing 10 μM $ZnSO_4$ at λ_{ex} 420 nm. The dotted lines represent the probe only spectrum while the solid lines represent the fluorescence spectrum of probe with 3 equiv of NDM-1.

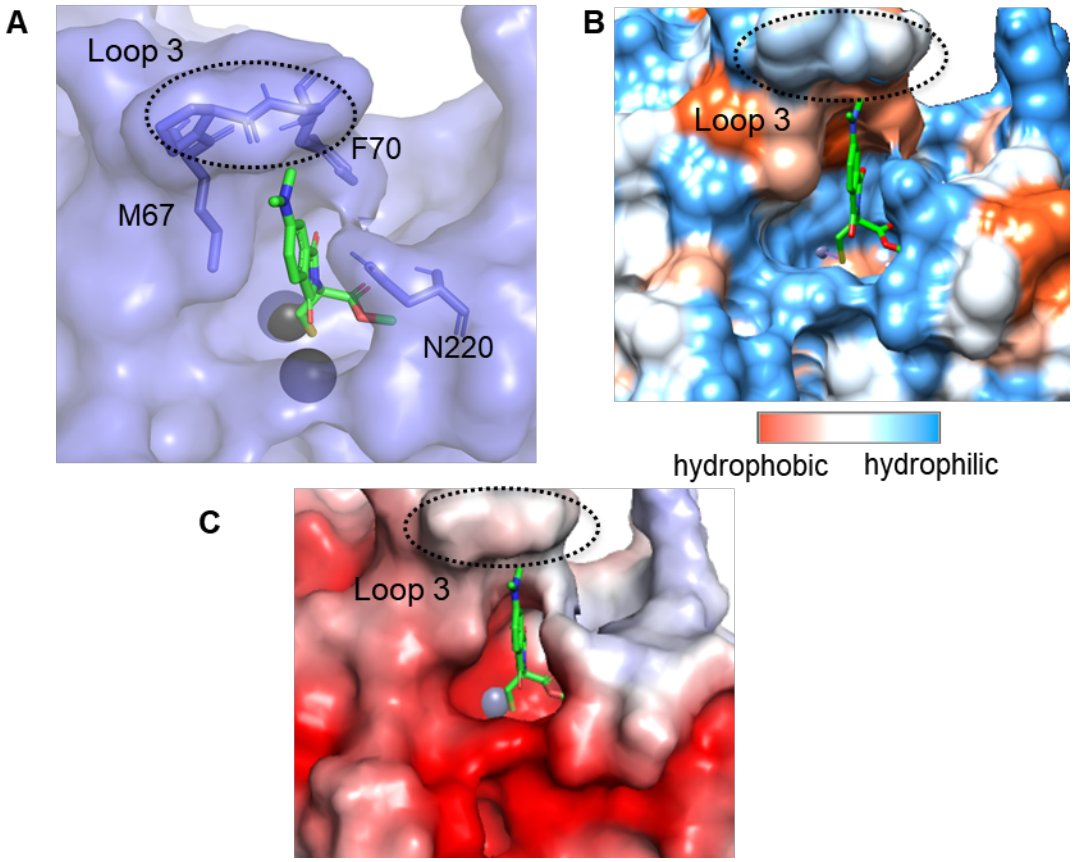

Fig. S2. Proposed Binding mode of **4D** (A) Zoomed-in view showing Loop 3 and the residues around the fluorophore end for probe **4D** in the modeled NDM active site using QM/DMD simulations (see computational section below). (B) Surface hydrophobicity view for **4D**-NDM-1 generated using UCSF Chimera. (C) Surface electrostatics view for **4D**-NDM-1 generated using PyMOL. Loop 3 is shown as a dotted sphere in all the images.

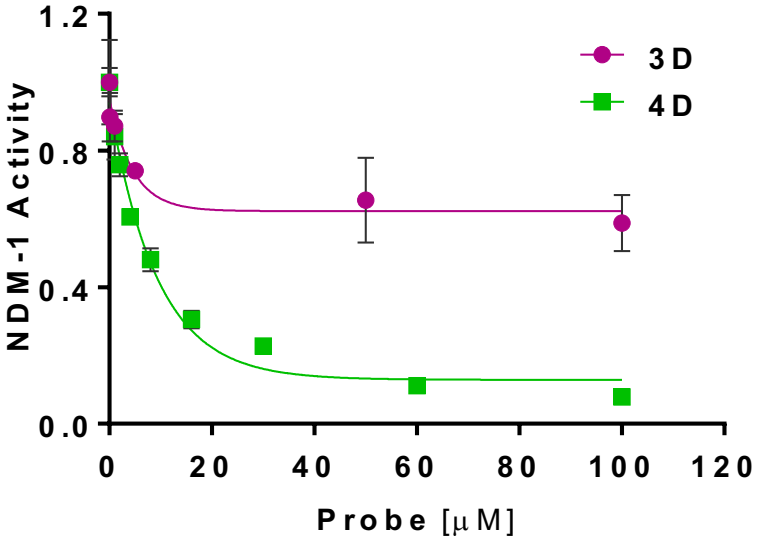

Fig. S3. IC_{50} plot for probes **3D** and **4D** with NDM-1 (20 nM) using chromacef (20 μM) as the substrate and 150 μM TCEP to avoid disulfide formation. The substrate hydrolysis rate was monitored at λ_{abs} 442 nm over 30 sec intervals. All studies were conducted in degassed 50 mM HEPES, pH 7.0 containing 10 μM $ZnSO_4$ at room temperature. The data was plotted on GraphPad Prism, with exponential one phase decay to obtain IC_{50} values. All probe stock solutions were made fresh every day in acetonitrile and kept on ice throughout the study to avoid disulfide formation. Apparent partial inhibition is observed by **3D** so this probe was discarded. Probe **4D** results in complete inhibition and was chosen for further study.

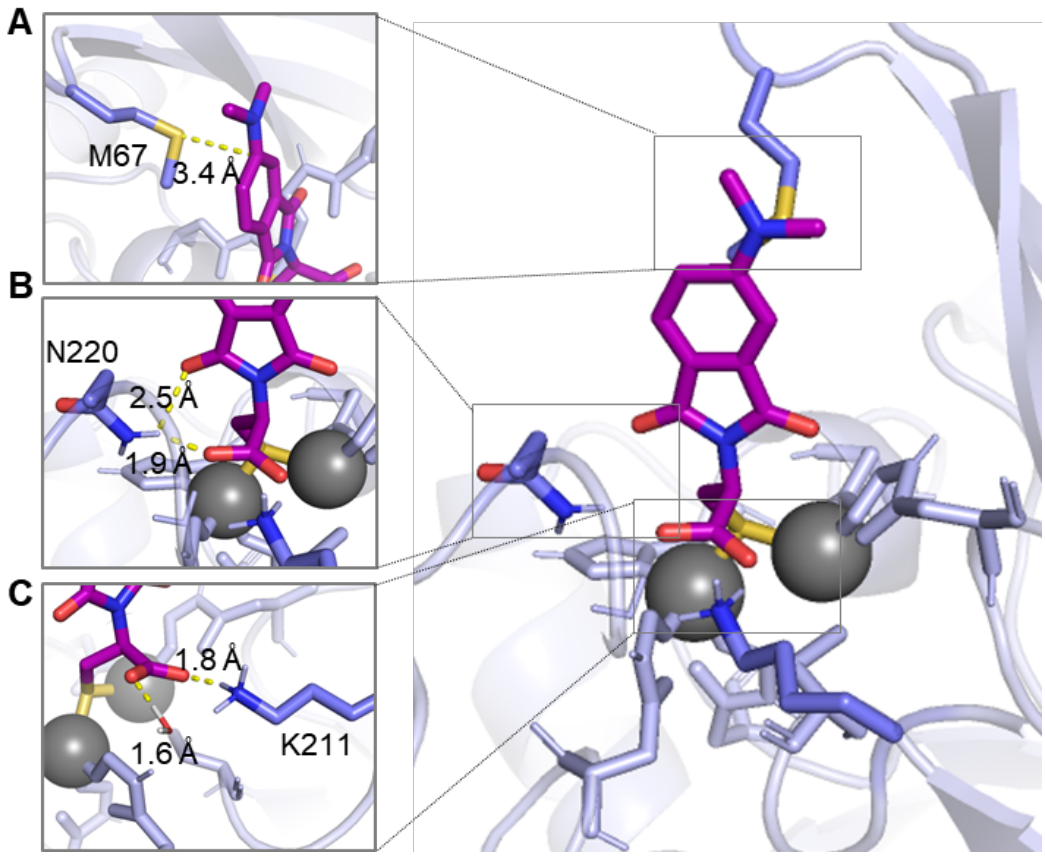

Fig. S4. Proposed binding modes from QM/DMD simulations for probe **3D** with NDM-1 (PDB: 4EXS) with insets showing (A) interactions between the fluorophore end of the probe and hydrophobic M67 in Loop 3. (B) Interaction between N220 and the carbonyl oxygen of the imide ring of the fluorophore. (C) Interaction between K211 and the carbonyl groups in the metal binding group end of the probe.

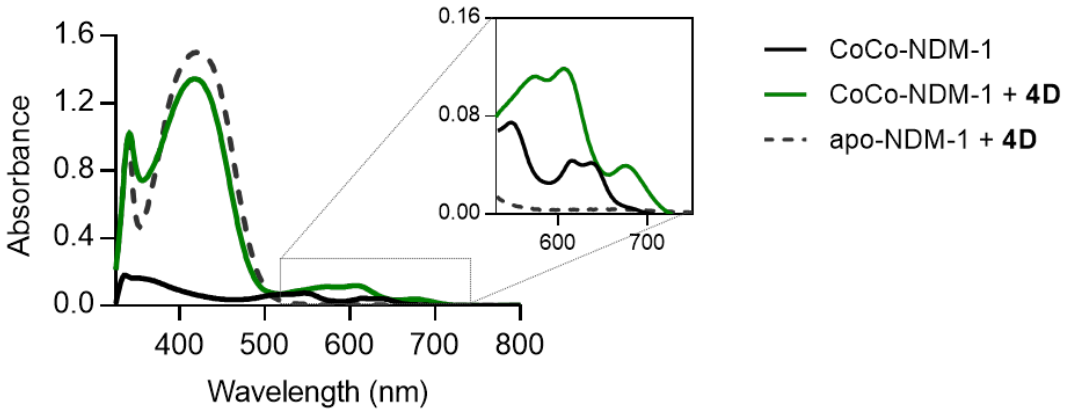

Fig. S5. UV-vis spectra of 300 μM CoCo-NDM-1 (black solid), CoCo-NDM-1 after incubation with 1 equivalent of **4D** (green solid), and metal-free NDM-1 after incubation with 1 equivalent of **4D** (grey dashed). The inset shows a zoomed-in view of the shift in d-d transitions upon probe binding. The buffer used in these spectra contained 50 mM HEPES, pH 6.8, 500 mM NaCl, 2 mM TCEP and 10% glycerol.

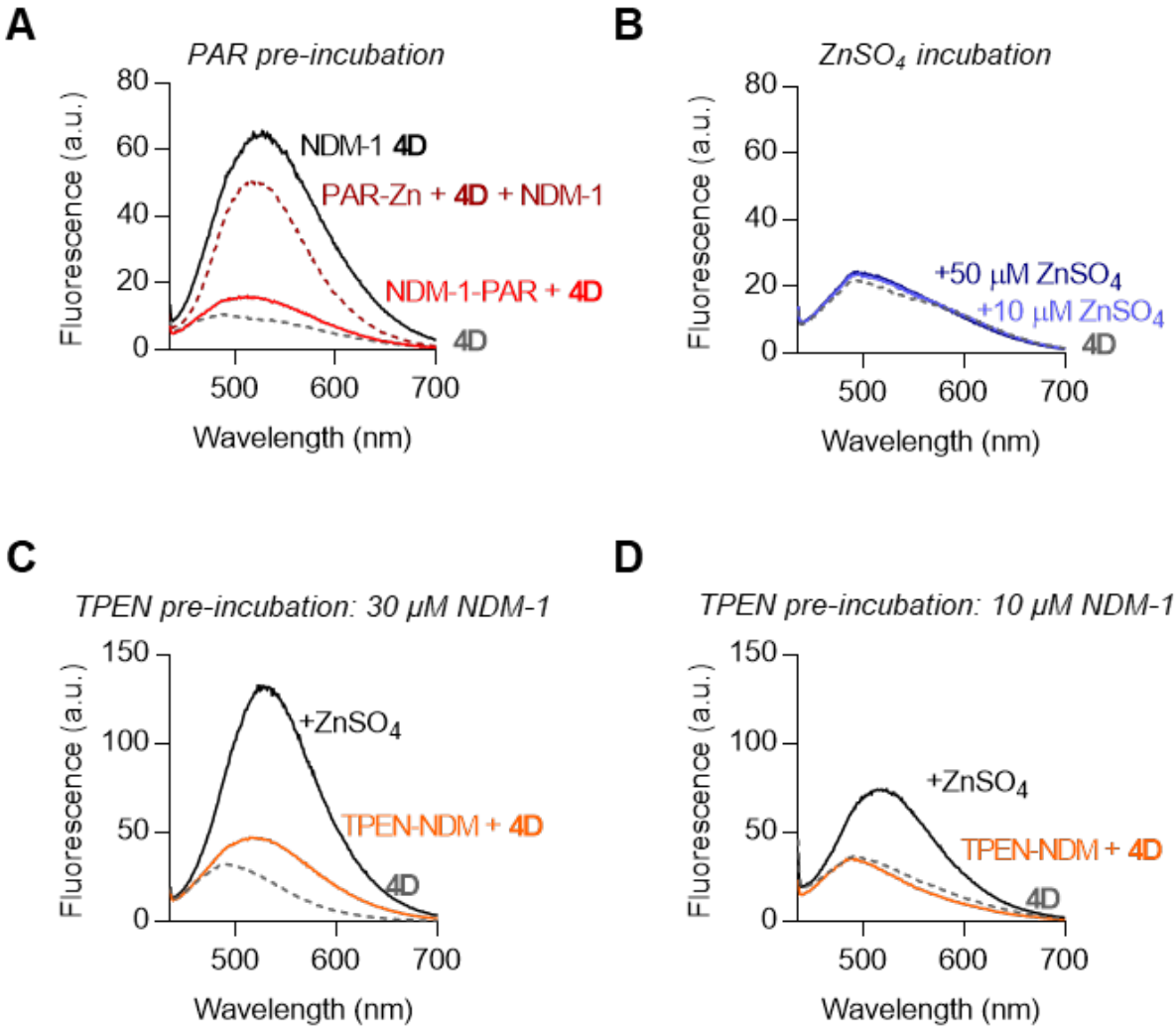

Fig. S6. (A) Difference in fluorescence response between **4D** (grey dashed line) vs **4D** incubated with NDM-1 (black line) or incubated with NDM-1 (10 μM) that was pre-treated with PAR (50 μM) (red line). While this observed decrease upon PAR incubation may in part be due to quenching by PAR-Zn complex (maroon dashed line), the overall intensity is still significantly lower in the sample with PAR-NDM (red solid line). (B) Incubation of probe **4D** with increasing concentrations of $ZnSO_4$ (blue) to denote no significant response with free Zn^{2+} in any studies. (C,D) Difference in fluorescence response upon pre-incubation (15 min incubation) of different amounts of NDM-1 with 50 μM TPEN showing a decrease in intensity upon **4D** addition (10 μM). It is interesting to note that at equimolar NDM-1 concentrations (10 μM), the fluorescence is completely quenched but is recovered in the presence of added $ZnSO_4$ (up to 50 μM). At 30 μM NDM-1 concentrations, the fluorescence is quenched to ~30% in the presence of 50 μM TPEN suggesting that in the presence higher equivalents of NDM-1, there is still some residual fluorescence due to NDM-1-**4D** interactions.

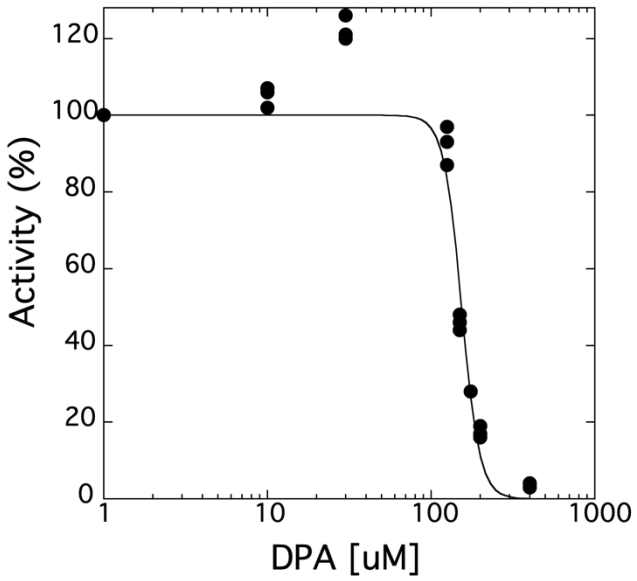

Figure S7. IC_{50} Value Determinations for NDM-1 Inhibition by Dipicolinic Acid in the Presence of Exogenous Zinc. In the presence of 50 μM $ZnSO_4$ and after a 20 min preincubation with NDM-1 (50 nM Δ35 NDM-1), dipicolinic acid inhibits chromacef (20 μM, $\Delta\varepsilon_{442}$ = 14,500 $M^{-1}cm^{-1}$, K_M = 0.66 μM[2, 7], Sopharmia, Platt City, MO) hydrolysis in a concentration-dependent manner (I), fitted (solid line) to give an IC_{50} = 154 ± 8 μM.

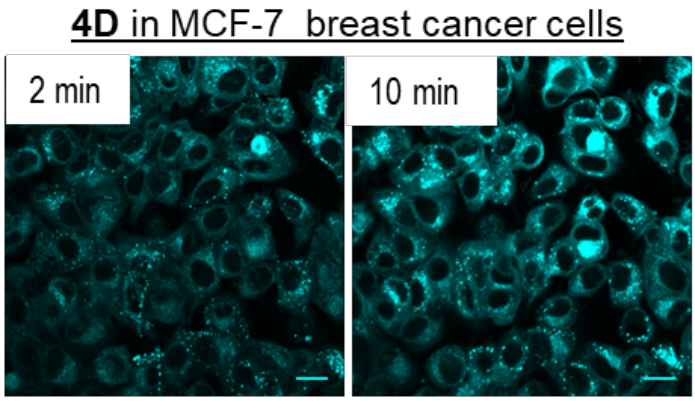

Fig. S8. Treatment of MCF-7 cells with probe **4D** resulted in a huge fluorescence turn-on within 10 min of incubation. (Scale: 10 μm; $\lambda_{ex}/\lambda_{em}$: 405/ 486-614).

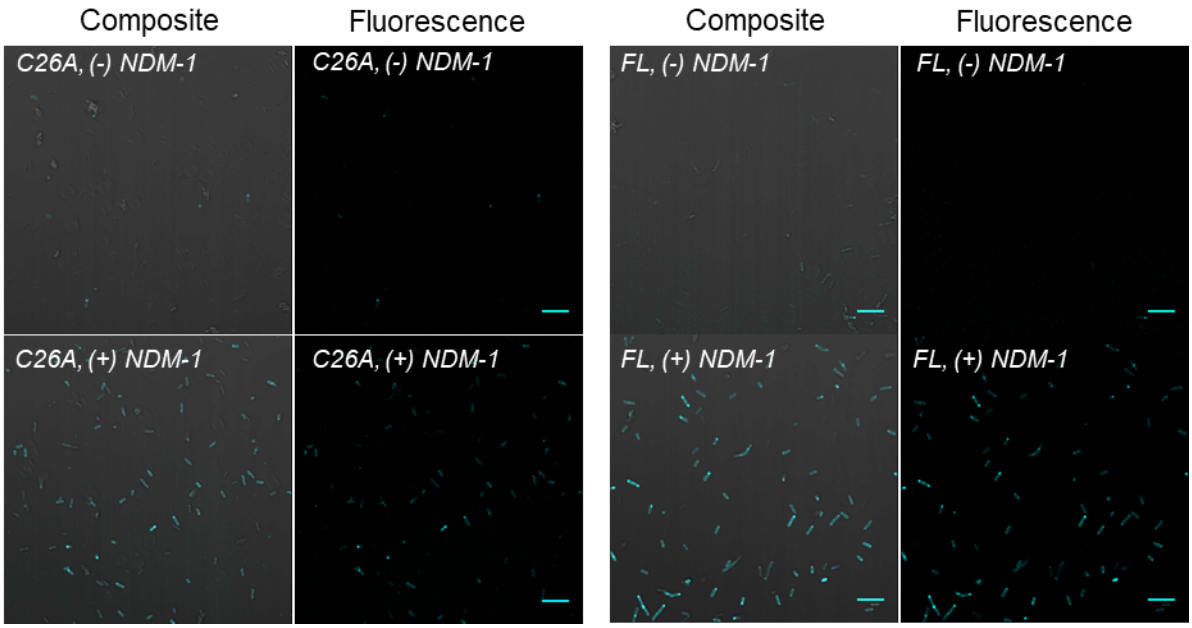

Fig. S9. Confocal imaging of **4D** treated *E. coli* BL21 (DE3) cells with the C26A and FL construct in the absence (-) and presence (+) of IPTG to induce NDM-1 expression.

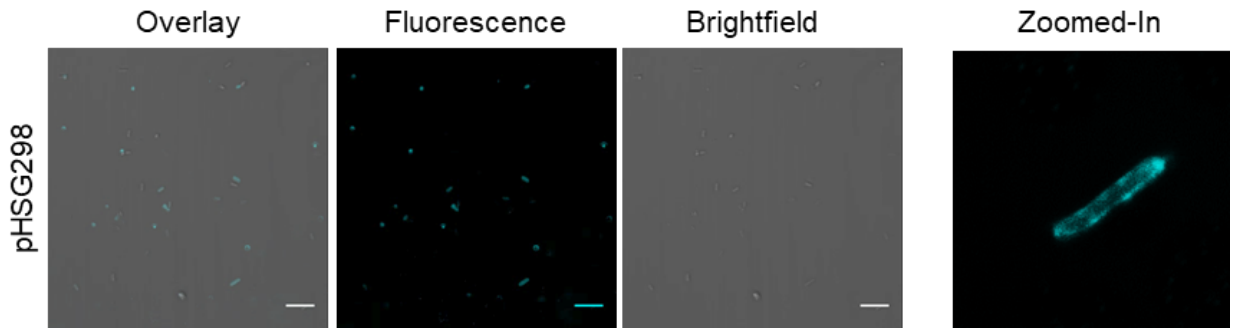

Fig. S10. Confocal imaging of **4D** treated *E. coli* DH5α cells with the pHSG298 vector that includes the native bla_{NDM} promoter and encodes full length NDM-1, including the lipidation signal (lipobox), to better mimic natural levels of NDM-1 expression. Zoomed-in view to observe fluorescence localization in the periplasmic region. Scale bar: 10 microns.

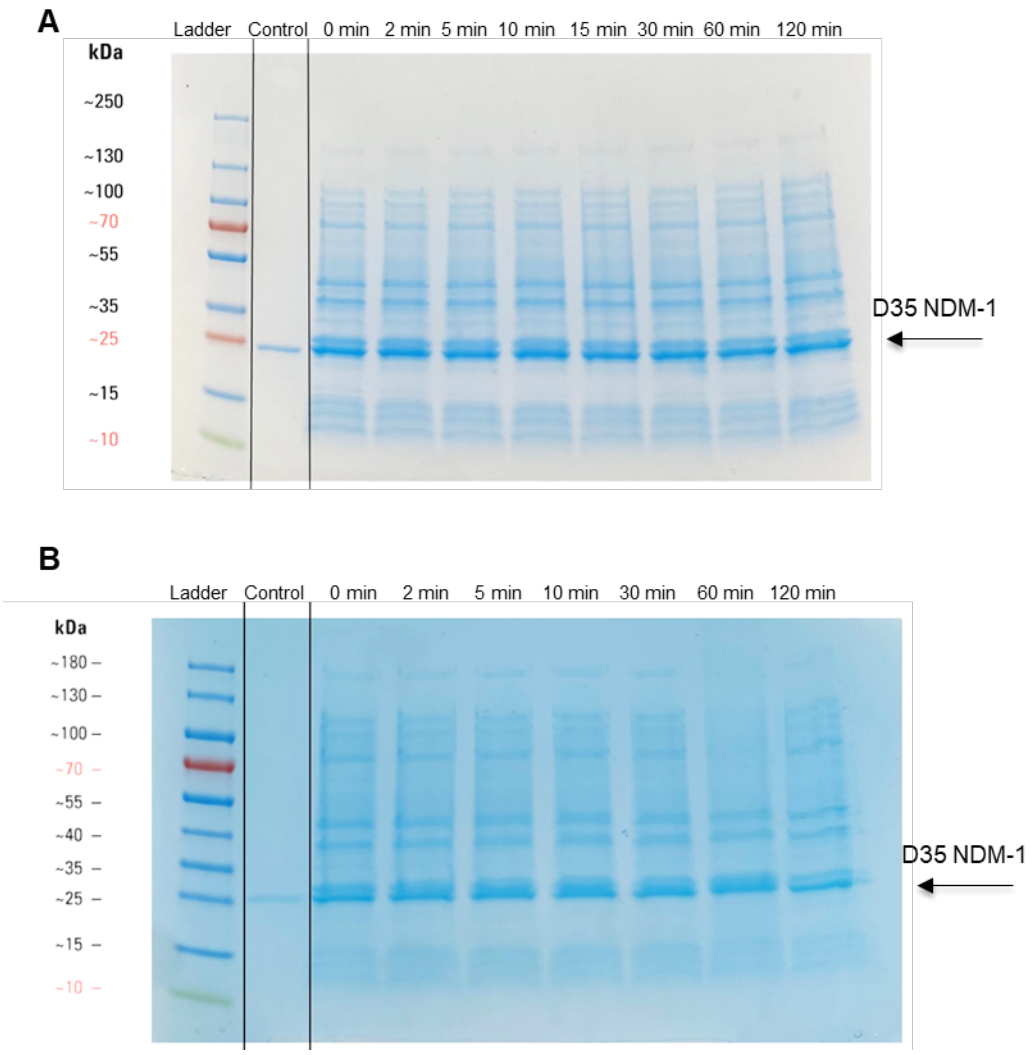

Fig. S11. SDS-PAGE of whole cell lysates at successive time points. *E. coli* BL21 (DE3) (pET27b-NDM1-Δ35) cells were cultured and induced as described for the imaging experiments in Fig. 5. After 1 h of expression, cells were pelleted and resuspended in M9 minimal media and supplemented (B) or not supplemented (A) with the cephalexin substrate (1 mM). Cells were incubated at 25 °C and aliquots removed at the successive time points indicated above each lane, mixed with loading buffer, boiled (5 min) and cooled before separation using a 4-20% Mini-Protein TGS (Biorad) stacking gradient SDS-PAGE gel stained with Coomassie stain to visualize protein bands. A prominent band was observed corresponding to that expected for Δ 35 NDM-1 and the intensity did not significantly vary over the time course used for the imaging experiments (typically < 60 min).

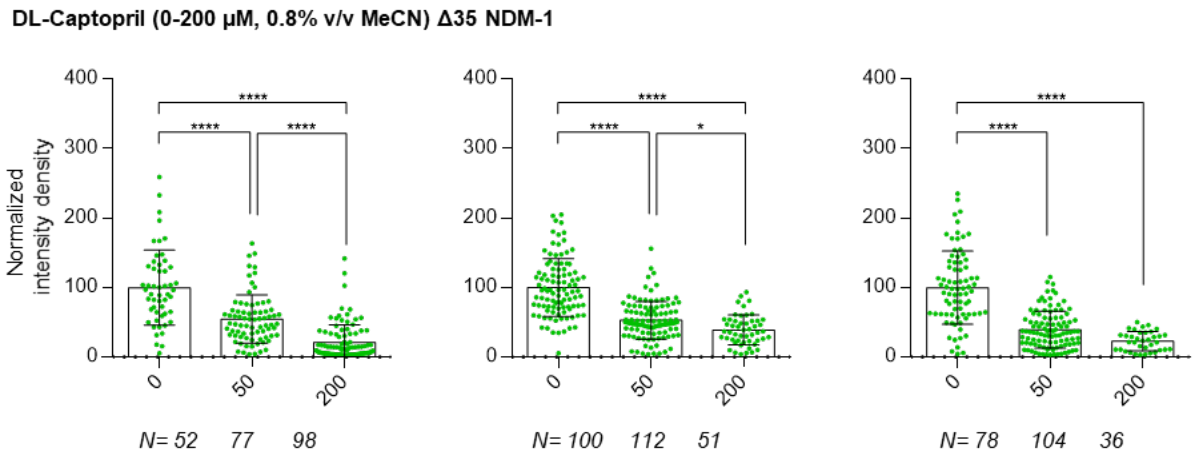

Fig. S12. Normalized intensity density for **4D** incubated *E. coli* BL21 (DE3) cells treated with varying concentrations of DL-captopril after expressing Δ35 NDM-1. The intensities were normalized to the 0 µM in each set. The green dots signify intensity per cell with the number of cells mentioned below each column. These graphs represent intensity data recorded over 3 different trials to ensure reproducibility. All data was analyzed using one-way ANOVA (* $p < 0.05$, ** $p < 0.01$, *** $p < 0.001$, **** $p < 0.0001$).

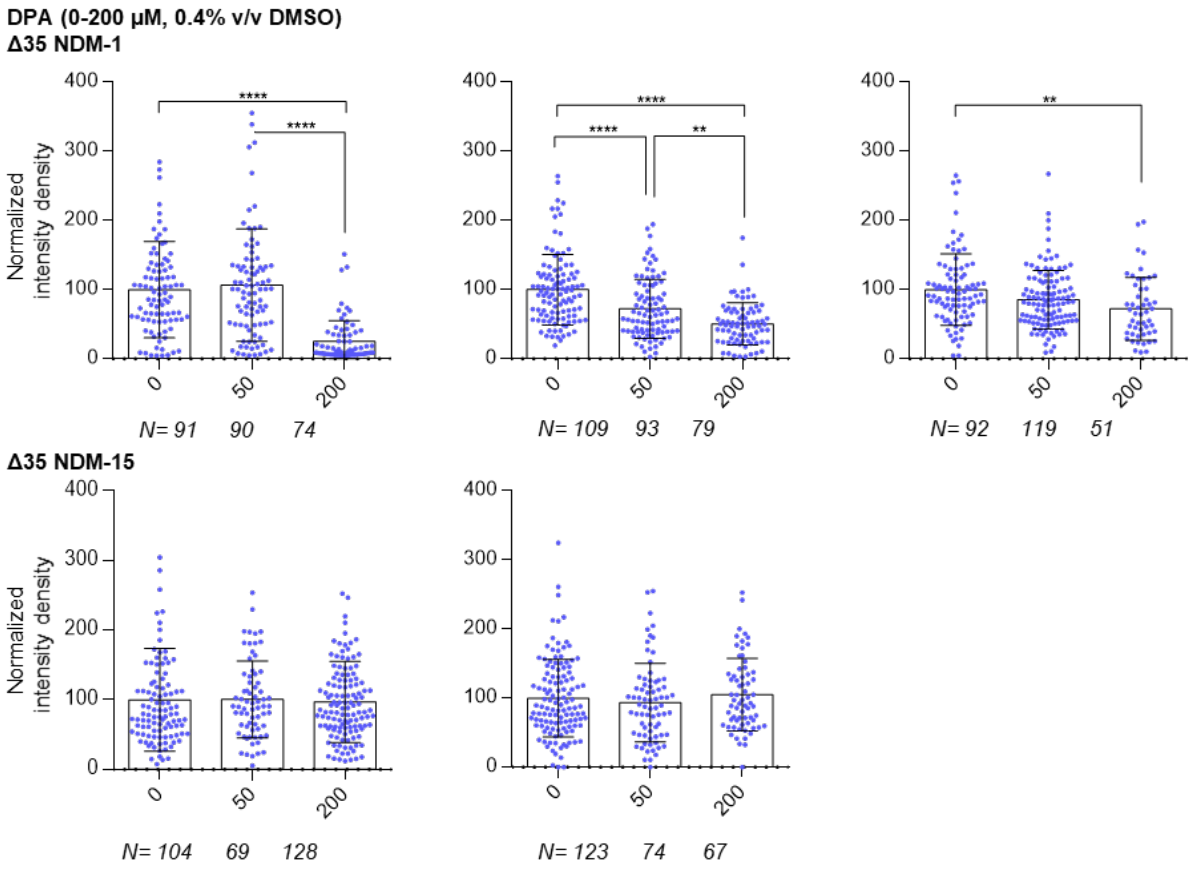

Fig. S13. Normalized intensity density for **4D** incubated *E. coli* BL21 (DE3) cells treated with varying concentrations of DPA after expressing Δ35 NDM-1 or NDM-15, respectively. The intensities were normalized to the 0 µM in each set. The blue dots signify intensity per cell with the number of cells mentioned below each column. These graphs represent intensity data recorded over 2-3 different trials to ensure reproducibility. All data was analyzed using one-way ANOVA (* $p < 0.05$, ** $p < 0.01$, *** $p < 0.001$, **** $p < 0.0001$).

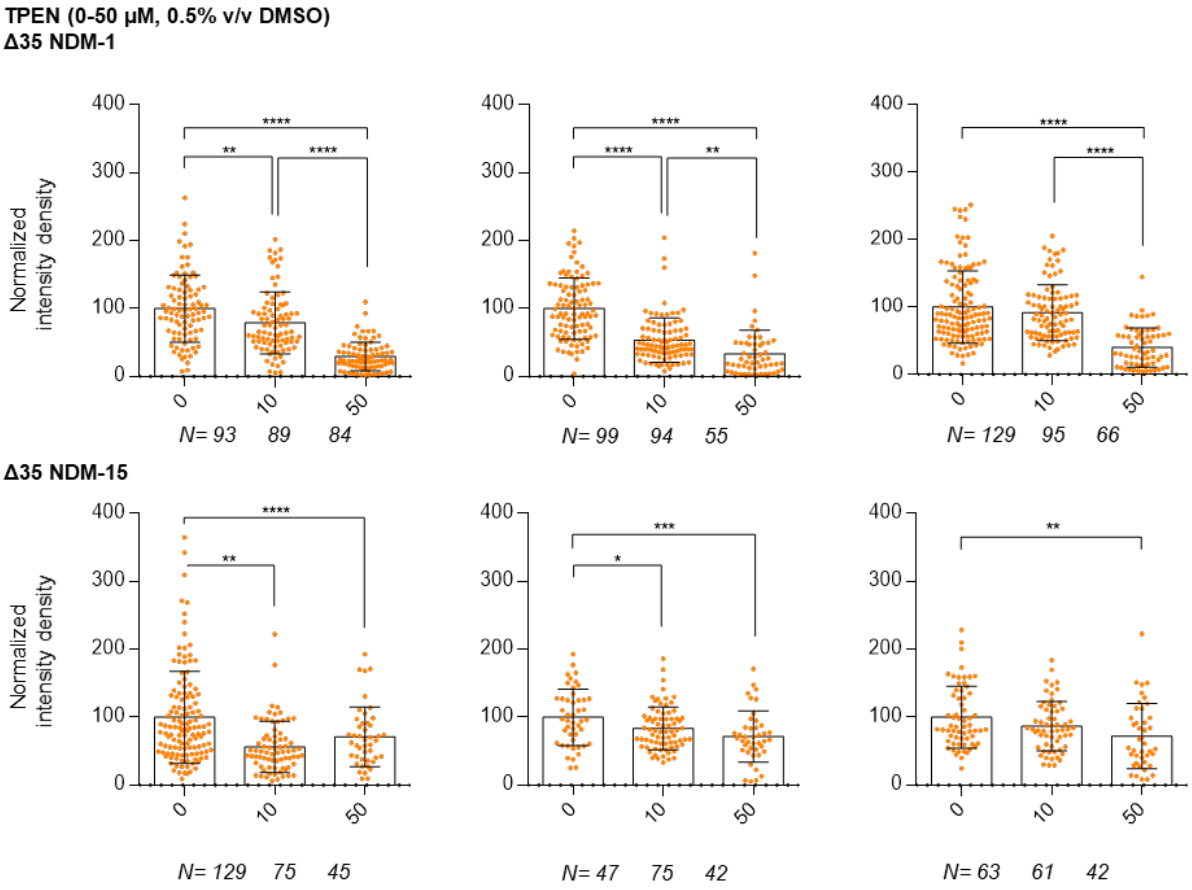

Fig. S14. Normalized intensity density for **4D** incubated *E. coli* BL21 (DE3) cells treated with varying concentrations of TPEN after expression of Δ35 NDM-1 or NDM-15, respectively. The intensities were normalized to the 0 µM in each set. The orange dots signify intensity per cell with the number of cells mentioned below each column. These graphs represent intensity data recorded over 3 different trials to ensure reproducibility. All data was analyzed using one-way ANOVA (* $p < 0.05$, ** $p < 0.01$, *** $p < 0.001$, **** $p < 0.0001$).

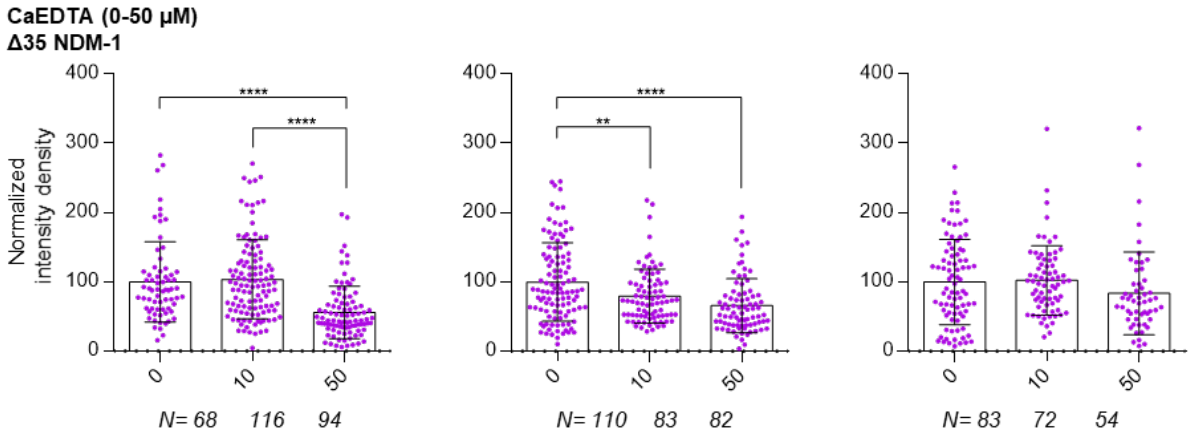

Fig. S15. Normalized intensity density for **4D** incubated *E. coli* BL21 (DE3) cells treated with varying concentrations of CaEDTA after expression of Δ35 NDM-1. The intensities were normalized to the 0 µM in each set. The purple dots signify intensity per cell with the number of cells mentioned below each column. These graphs represent intensity data recorded over 3 different trials to ensure reproducibility. All data was analyzed using one-way ANOVA (* $p < 0.05$, ** $p < 0.01$, *** $p < 0.001$, **** $p < 0.0001$).

General Computational Methods and Additional Analyses

General Computational Methods

The computational results are based off structures and energies generated by the QM/DMD method.[8] This approach is a form of molecular dynamics simulation specialized for metalloproteins that couples the quantum mechanical (QM) treatment necessary to treat the metal centers and their coordination with rapid discrete molecular dynamics (DMD) sampling of the rest of the protein. Both methods treat an overlapping QM/DMD region, which consists of species participating in relevant, non-covalent interactions about the metal, to enable inter-region communication and reduce discontinuity errors. QM/DMD has been used to successfully study a range of metalloenzyme behaviors, including protein metal affinity,[9-11] flexible docking to metalloenzymes,[12] and metal-dependent catalytic activity.[13, 14] Density functional theory (DFT) was used here as the quantum mechanical method. A total of 18 QM/DMD simulations were run for this study, consisting of three replicate calculations for every binding mode (1-3) of both probes (**3D** and **4D**). A crystal structure of NDM-1 (PDB ID: 4EXS[15]) was adapted for the simulations. All simulations were run for 20 iterations, equivalent to approximately 10 ns of sampling. Free energies were obtained through additional DFT harmonic frequency calculations of QM/DMD structures. The simulation system construction, full details of the methodology used, and verification of simulation convergence are discussed below.

Computational Analysis of the Preferred Binding Mode

Three binding modes for both probes were considered with QM/DMD simulations. These are the probe thiol and ester/carboxylate binding the metals together with the oxygen on the histidine bound zinc – referred to as mode 1, thiol and ester/carboxylate dual binding but with the sulfur on the histidine bound zinc – mode 2, and ester/carboxylate solely binding to both metals – mode 3. Within a couple of QM/DMD iterations all of these initial binding geometries are rejected in favor

of thiol binding between the two zinc centers in the same manner as L-Captopril. In the cases of mode 1 and mode 3, an oxygen of the ester/carboxylate group generally still coordinates one of the metal centers, while in the case of mode 2 this group interacts directly or indirectly with K211 instead. Of the equilibrated binding arrangements, mode 2 is greatly preferred in energy over the other two for probes **3D** and **4D**. For probe **3D**, the lowest QM region free energies are 23.8 and 17.8 kcal/mol above that of mode 2 for modes 1 and 3 respectively. These values are 21.7 and 9.1 kcal/mol above for modes 1 and 3 in **4D**. All other analyses of the computational results are based on the mode 2 simulations, as they are significantly lower in energy.

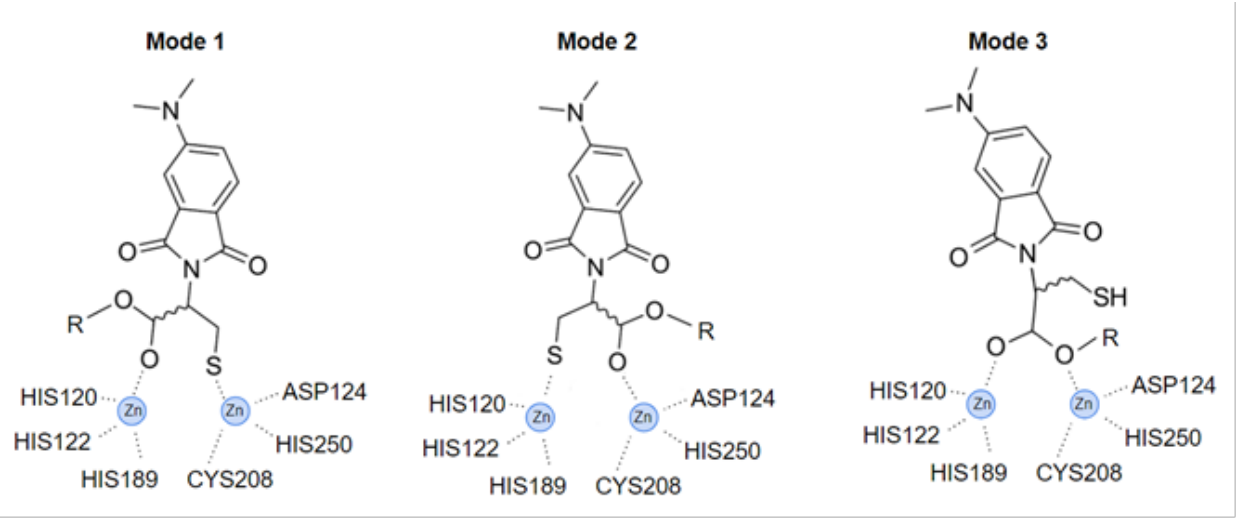

Fig. S16. Input probe binding mode geometries, showing the initial coordination to the metal centers. R is either H (**3D**) or CH_3 (**4D**).

*Further Computational Analysis of Non-Covalent Interactions with **3D** and **4D** Probes*

In the analysis of QM/DMD results, consideration of the generated full ensemble of QM states is important. While the lowest energy structure according to QM is the single most significant and demands particular attention, the density of the full ensemble of states (assuming they are not so prohibitively high in energy) indicates entropic favorabilities that an individual structure does not account for. Given the vast conformational space accessible to any protein, the calculated QM energy for each structure is unable to take the full entropy of the system into account.

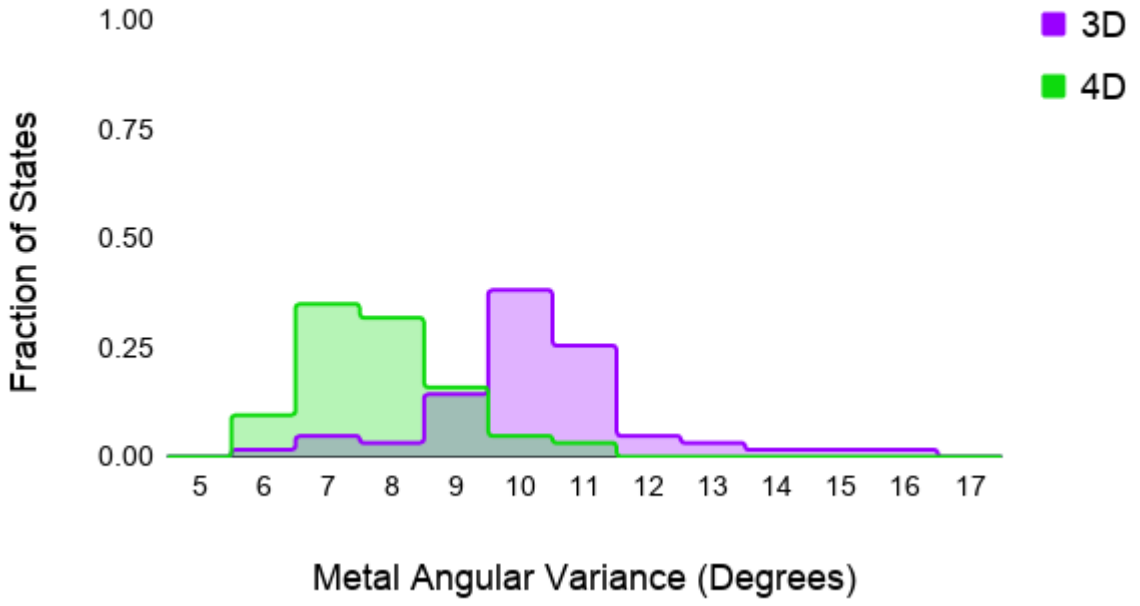

Fig. S17. Histogram of the metal angle variance for each optimized QM structure from QM/DMD for **3D** and **4D**. The values are binned in 1 degree increments. Notice how the bulk of the metal angle variances are lower for **4D** than **3D**.

Analysis of the full ensemble of states for probes **3D** and **4D** with respect to the metal angle variance shows **4D** adopts more ideal and stable geometries. The plot shows the peak for the **4D** population around 7 – 9° and the peak for the **3D** population around the higher 10 – 11°. This means that **4D** adopts metal geometries closer to the ideal and most stable tetrahedral geometry for zinc, which contributes to stronger binding.

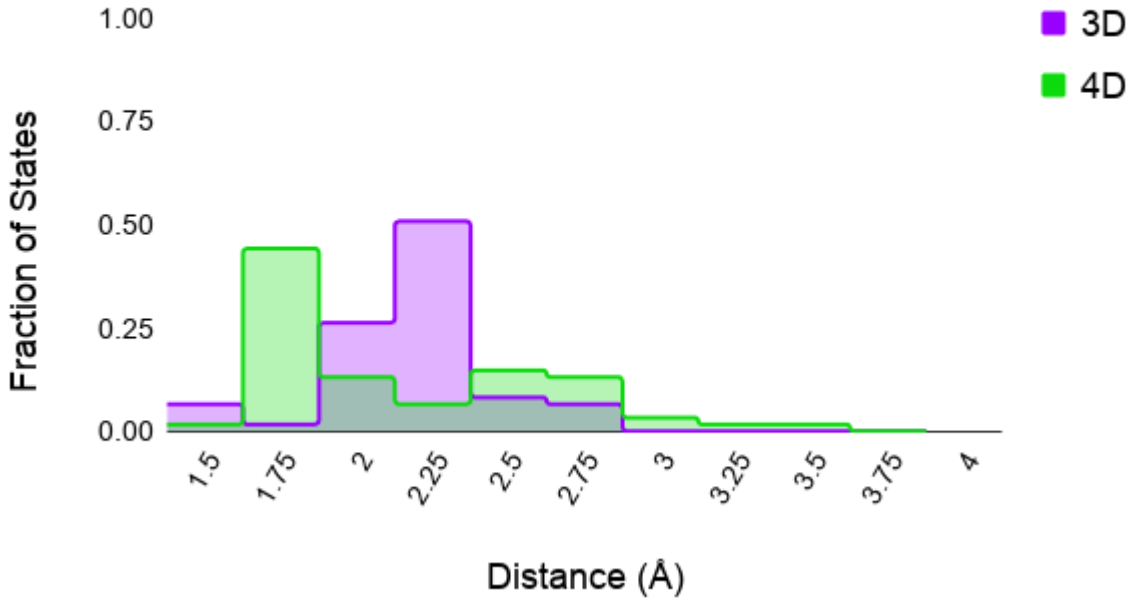

Fig. S18. Histogram of K211-probe distance across all QM optimized structures for both **3D** (purple) and **4D** (green). The distance represents the minimum one between each K211 amine hydrogen and both oxygen in the probe ester/carboxylate for each structure. Distances are binned in 0.25 Å intervals, starting at 1.5 Å. Distances around 2 Å and below correspond to a hydrogen bonding interaction, while those above are not, or involve a water intermediary. Note that probe **4D** frequently adopts a hydrogen bond directly to K211, while **3D** rarely does.

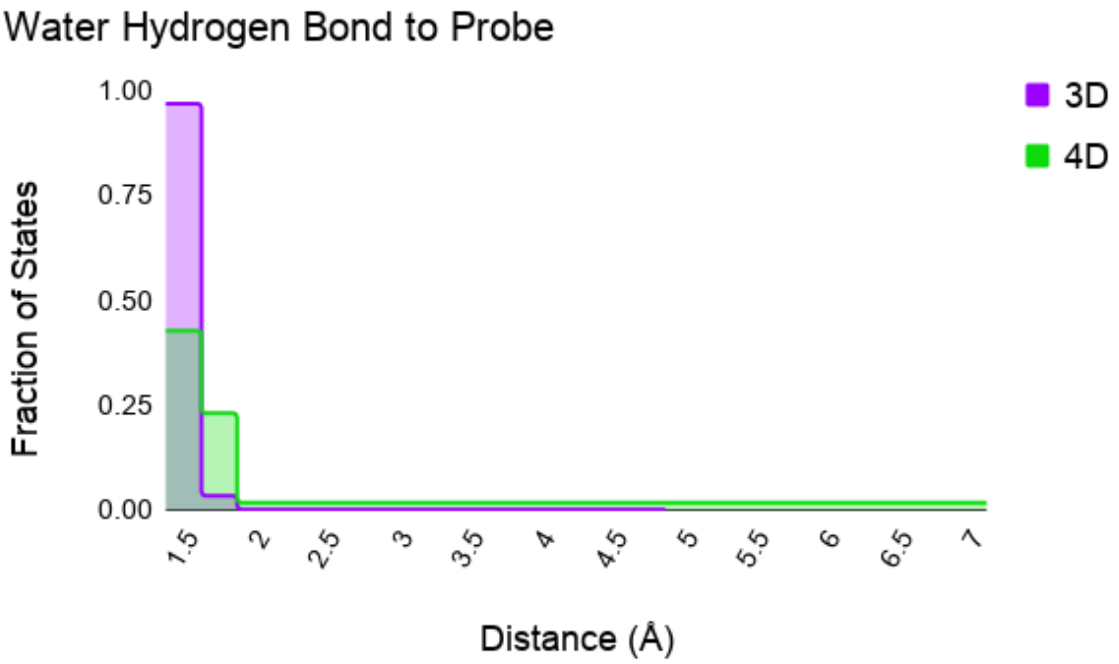

Fig. S19. Histogram of explicit water-probe distance across all QM optimized structures for both **3D** (purple) and **4D** (green). The distance represents the minimum one between each K211 amine hydrogen and the oxygen of the explicitly modeled water for each structure. Distances are binned in 0.25 Å intervals, starting at 1.5 Å. Notice that a hydrogen bond to water is nearly always adopted by both probes, though this interaction is more often longer and weaker in **4D**.

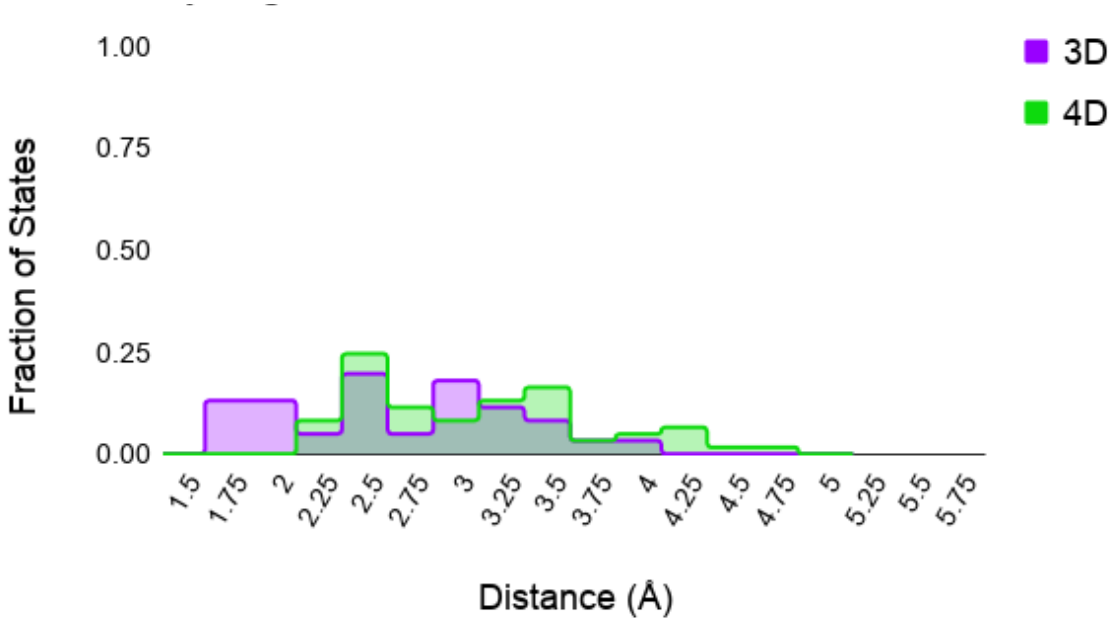

Fig. S20. Histogram of N220-probe distance across all QM optimized structures for both **3D** (purple) and **4D** (green). The distance represents the minimum one for each structure between each N220 hydrogen on the amide nitrogen and both carbonyl oxygen on the probe ring. Distances are binned in 0.25 Å intervals, starting at 1.5 Å. Distances around 2 Å and below correspond to a hydrogen bonding interaction, which sometimes occurs for **3D**, but never for **4D**. Note that there is no significant peak around this hydrogen-bonding interaction for **3D** as is the case for the K211-probe direct hydrogen bonding contact in **4D**.

Analysis of non-covalent QM-region interactions in the ensembles of probes **3D** and **4D** show critical differences that may explain the tighter binding of **4D**. Plotting the hydrogen-oxygen distance between K211 amine and the probe ester/carboxylate group shows that **4D** adopts a direct hydrogen bond much more readily than **3D**. Its peak from 1.75 – 2 Å matches the characteristic hydrogen bond length, while the **3D** peak from 2 – 2.5 Å represents an interaction instead mediated by a water molecule. While **3D** does occasionally adopt a direct hydrogen bond between K211 and the probe, this is rare. A graph of the hydrogen-oxygen distance between the K211 amine and the QM region water molecule shows that a hydrogen bond between these species is nearly always present for both **3D** and **4D**. This interaction is typically in lieu of a direct

K211-probe interaction for **3D**, while it is typically in conjunction with a direct interaction for **4D**. Instead, **3D** seems to more frequently form a hydrogen bonding interaction between the probe and N220. A plot of the hydrogen-oxygen distance between the N220 amide and probe ring carbonyls shows regular adoption of a distance around 2 Å and below for **3D**, while this situation was never the case for **4D**. As this is still much less common than the direct K211-probe interaction in **4D**, the entropic favorability of that interaction could explain the slightly tighter binding of **4D** to NDM-1 over **3D**, and therefore its better inhibition.

Simulation System Construction

All simulations were based on a crystal structure of NDM-1 bound to L-captopril (PDB ID: 4EXS). One of the monomers (chain B) and all water molecules except one near K211 were removed from the structure. The captopril was removed with the appropriate probe installed in its place (**3D** or **4D**). Three binding modes were assessed, with the initial position of the probe selected accordingly. The initial geometries for each binding mode are shown. The region treated with QM included the probe, metals, the full side chains of M67, W93, H120, H122, D124, H189, C208, K211, N220, and H250 starting from the beta carbon and an additional water molecule positioned near K211 that forms a hydrogen bond with it in the original crystal structure.

Full Computational Methodological Details

QM/DMD simulations[8] are run in an iterative fashion, alternating from a DMD simulation[16] of the protein to a QM geometry optimization. All DMD phases were performed for 10,000 steps per iteration (approximately 0.5 ns). These simulations run with an implicit solvent through potentials specified in its force field. As stated in the main body of this article, DFT was used for all QM calculations with Turbomole (version 6.6). The pure meta-GGA TPSS functional[17] was used with the D3 dispersion correction.[18] The metal was treated with the triple-zeta basis set def2-TZVPP and all other atoms with the double zeta def2-SVP basis set.[19] While the small basis set may result in some degree of basis set superposition error, the large size of the QM regions have precluded the use of larger basis sets. Furthermore, the level of theory employed has proven effective in the past studies, cited in the main article and earlier in the SI. The Conductor-like Screen Model (COSMO) with a constant dielectric of 20 was applied to approximate the screening and solvation effects in the partially buried NDM-1 probe binding site.[20] A water molecule involved in important hydrogen bonding with K211 was included explicitly. All QM calculations were performed to full convergence within 1.0×10^{-6} Hartree. Free energies were obtained from numerical harmonic frequency calculations on converged DFT structures using the same level of theory as the geometry optimizations.

Probe binding penalties were calculated by comparing the free energy of the probe geometry adopted in the lowest energy NDM-1 bound structure from QM/DMD to its geometry adopted in solution. This was done by calculating the free energy difference between of the probe removed from the QM region which was quickly geometry optimized with all heavy atoms frozen and the fully relaxed structure after a geometry optimization without any structural constraints. The QM methodology used was the same as above for the QM/DMD simulations, but with a COSMO dielectric of 80 for the fully solvent relaxed structure to represent the aqueous environment.

Metal angle variance was calculated using the equation $\sigma_{tet} = \frac{1}{6}\sum_{i=1}^{6}|\theta_i - 109.5^{o}|$ which sums the deviation of each of the 6 characteristic angles from the ideal 109.5° for a tetrahedral geometry. This is demonstrated in the figure below.

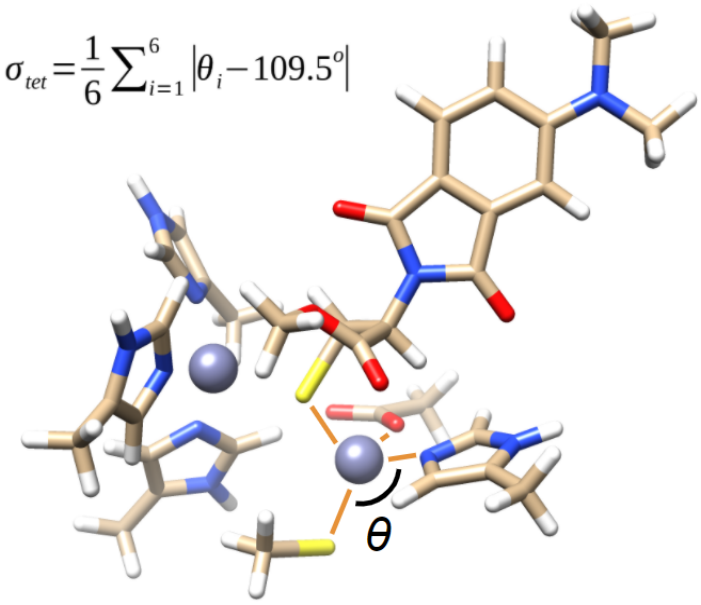

Fig. S21. Example of a metal angle variance calculation for one of the zinc centers of NDM-1. The variance is based on each of the inscribed angles between the metal-ligand bonds (in orange). The variance of the other metal is calculated in the same fashion.

Verification of Simulation Convergence

Convergence was tracked through the backbone RMSD (calculated with respect to the alpha carbon and amide carbon, nitrogen, and oxygen of each amino acid residue), QM energy, and DMD energy. All RMSD values were calculated using the initial protein equilibrated for one QM/DMD iteration as the reference frame. The QM and DMD energies are plotted relative to the lowest energy value for each probe. The trajectory for these quantities are plotted below for each simulation. The graphs show gradual convergence, with oscillations around a steady value observed by the end of each simulation.

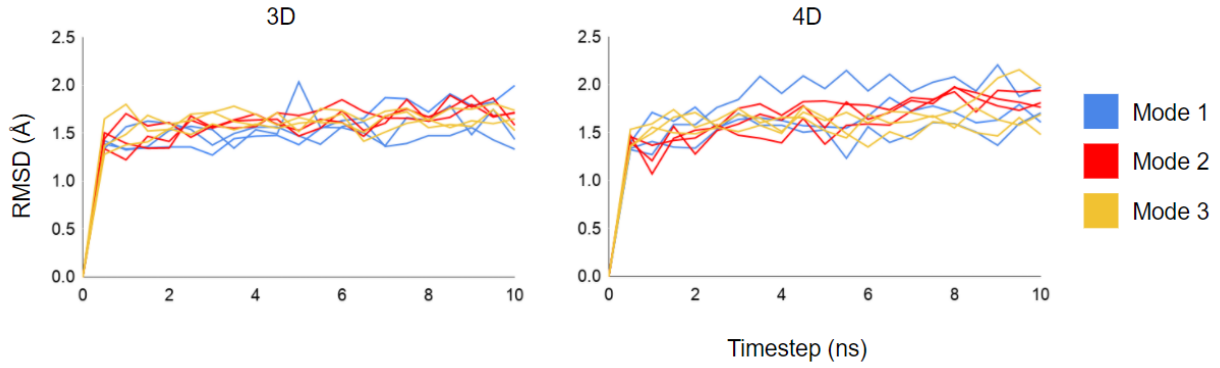

Fig. S22. Backbone RMSD trajectories for each QM/DMD simulation. All trajectories demonstrate convergence by oscillating around 1.5 Å to 2.0 Å.

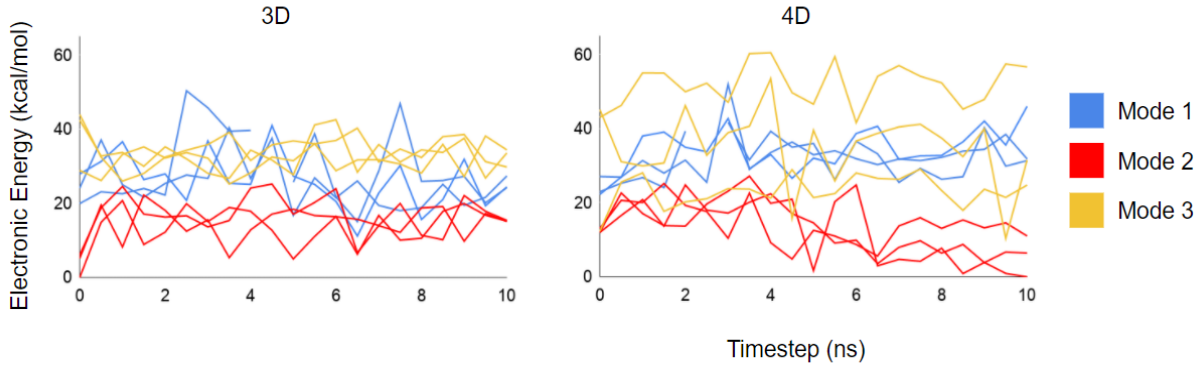

Fig. S23. QM optimized electronic energies for each QM/DMD simulation. Energies are relative to the lowest energy structure for each probe (regardless of binding mode). All trajectories for each mode tend to oscillate around a fixed value, showing convergence. Also note how that the mode 2 energies are generally lower than the others.

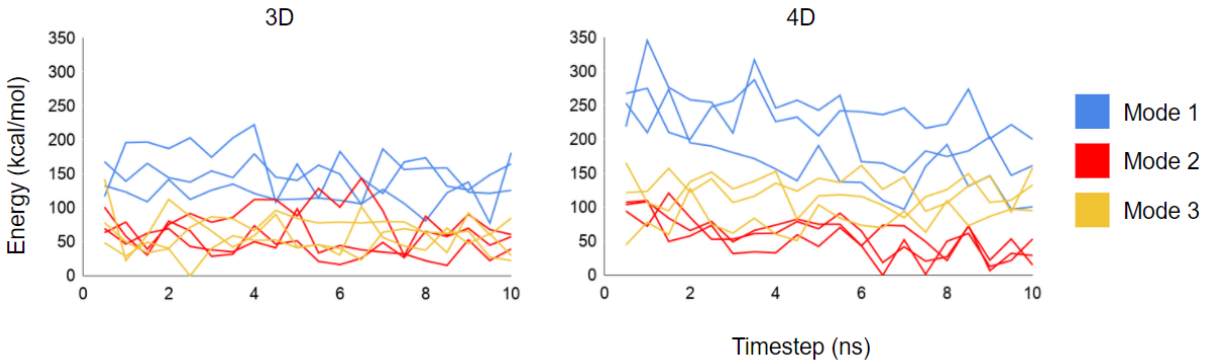

Fig. S24. DMD energies for each QM/DMD simulation. Energies are relative to the lowest energy structure for each probe (regardless of binding mode). These show convergence as each trajectory oscillates about a stable value by the end of the simulation. Again, note that the energies for mode 2 are generally lower than those of the other modes.

References

1. Mehta, R.; Qureshi, M. H.; Purchal, M. K.; Greer, S. M.; Gong, S.; Ngo, C.; Que, E. L., A new probe for detecting zinc-bound carbonic anhydrase in cell lysates and cells. *Chem Commun (Camb)* **2018,** *54* (43), 5442-5445.
2. Yu, S.; Vosbeek, A.; Corbella, K.; Severson, J.; Schesser, J.; Sutton, L. D., A chromogenic cephalosporin for β-lactamase inhibitor screening assays. *Analytical biochemistry* **2012,** *428* (2), 96-98.
3. Nowakowski, A. B.; Wobig, W. J.; Petering, D. H., Native SDS-PAGE: high resolution electrophoretic separation of proteins with retention of native properties including bound metal ions. *Metallomics* **2014,** *6* (5), 1068-78.
4. Thomas, P. W.; Zheng, M.; Wu, S.; Guo, H.; Liu, D.; Xu, D.; Fast, W., Characterization of Purified New Delhi Metallo-β-lactamase-1. *Biochemistry* **2011,** *50* (46), 10102-10113.
5. Stewart, A. C.; Bethel, C. R.; VanPelt, J.; Bergstrom, A.; Cheng, Z.; Miller, C. G.; Williams, C.; Poth, R.; Morris, M.; Lahey, O.; Nix, J. C.; Tierney, D. L.; Page, R. C.; Crowder, M. W.; Bonomo, R. A.; Fast, W., Clinical Variants of New Delhi Metallo-β-Lactamase Are Evolving To Overcome Zinc Scarcity. *ACS Infect Dis* **2017,** *3* (12), 927-940.
6. Cheng, Z.; Thomas, P. W.; Ju, L.; Bergstrom, A.; Mason, K.; Clayton, D.; Miller, C.; Bethel, C. R.; VanPelt, J.; Tierney, D. L.; Page, R. C.; Bonomo, R. A.; Fast, W.; Crowder, M. W., Evolution of New Delhi metallo-β-lactamase (NDM) in the clinic: Effects of NDM mutations on stability, zinc affinity, and mono-zinc activity. *J Biol Chem* **2018,** *293* (32), 12606-12618.
7. Chen, A. Y.; Thomas, P. W.; Stewart, A. C.; Bergstrom, A.; Cheng, Z.; Miller, C.; Bethel, C. R.; Marshall, S. H.; Credille, C. V.; Riley, C. L.; Page, R. C.; Bonomo, R. A.; Crowder, M. W.; Tierney, D. L.; Fast, W.; Cohen, S. M., Dipicolinic Acid Derivatives as Inhibitors of New Delhi Metallo-β-lactamase-1. *J Med Chem* **2017,** *60* (17), 7267-7283.
8. Sparta, M.; Shirvanyants, D.; Ding, F.; Dokholyan, N. V.; Alexandrova, A. N., Hybrid dynamics simulation engine for metalloproteins. *Biophysical journal* **2012,** *103* (4), 767-776.
9. Reilley, D. J.; Hennefarth, M. R.; Alexandrova, A. N., The Case for Enzymatic Competitive Metal Affinity Methods. *ACS Catalysis* **2020,** *10* (3), 2298-2307.
10. Reilley, D. J.; Fuller, J. T., 3rd; Nechay, M. R.; Victor, M.; Li, W.; Ruberry, J. D.; Mujika, J. I.; Lopez, X.; Alexandrova, A. N., Toxic and Physiological Metal Uptake and Release by Human Serum Transferrin. *Biophys J* **2020,** *118* (12), 2979-2988.
11. Nechay, M. R.; Gallup, N. M.; Morgenstern, A.; Smith, Q. A.; Eberhart, M. E.; Alexandrova, A. N., Histone Deacetylase 8: Characterization of Physiological Divalent Metal Catalysis. *The Journal of Physical Chemistry B* **2016,** *120* (26), 5884-5895.
12. Valdez, C. E.; Sparta, M.; Alexandrova, A. N., The Role of the Flexible L43-S54 Protein Loop in the CcrA Metallo-β-lactamase in Binding Structurally Dissimilar β-Lactam Antibiotics. *Journal of Chemical Theory and Computation* **2013,** *9* (1), 730-737.
13. Valdez, C. E.; Alexandrova, A. N., Why Urease Is a Di-Nickel Enzyme whereas the CcrA β-Lactamase Is a Di-Zinc Enzyme. *The Journal of Physical Chemistry B* **2012,** *116* (35), 10649-10656.
14. Sparta, M.; Valdez, C. E.; Alexandrova, A. N., Metal-dependent activity of Fe and Ni acireductone dioxygenases: how two electrons reroute the catalytic pathway. *J Mol Biol* **2013,** *425* (16), 3007-18.

15. King, D. T.; Worrall, L. J.; Gruninger, R.; Strynadka, N. C., New Delhi metallo-β-lactamase: structural insights into β-lactam recognition and inhibition. *J Am Chem Soc* **2012,** *134* (28), 11362-5.
16. Ding, F.; Tsao, D.; Nie, H.; Dokholyan, N. V., Ab initio folding of proteins with all-atom discrete molecular dynamics. *Structure* **2008,** *16* (7), 1010-8.
17. Staroverov, V. N.; Scuseria, G. E.; Tao, J.; Perdew, J. P., Comparative assessment of a new nonempirical density functional: Molecules and hydrogen-bonded complexes. *The Journal of Chemical Physics* **2003,** *119* (23), 12129-12137.
18. Grimme, S.; Antony, J.; Ehrlich, S.; Krieg, H., A consistent and accurate ab initio parametrization of density functional dispersion correction (DFT-D) for the 94 elements H-Pu. *The Journal of Chemical Physics* **2010,** *132* (15), 154104.
19. Weigend, F.; Ahlrichs, R., Balanced basis sets of split valence, triple zeta valence and quadruple zeta valence quality for H to Rn: Design and assessment of accuracy. *Phys Chem Chem Phys* **2005,** *7* (18), 3297-305.
20. Klamt, A., Conductor-like Screening Model for Real Solvents: A New Approach to the Quantitative Calculation of Solvation Phenomena. *The Journal of Physical Chemistry* **1995,** *99* (7), 2224-2235.

Probe **1**

Target Compound Screening Report

Results Acquired by The University of Texas at Austin Mass Spectrometry Facility

Data File	MSF20-0980(DM-C2-SH (1))_hrESIpos2.d	**Sample Name**	0980(DM-C2-SH (1))	**Comment**	0980(DM-C2-SH (1))
Position	P1-A1	**Instrument Name**	Instrument 1	**User Name**	
Acq Method	FIA_pos.m	**Acquired Time**	9/25/2020 10:31:06 AM	**DA Method**	KS.m

MS Zoomed Spectrum

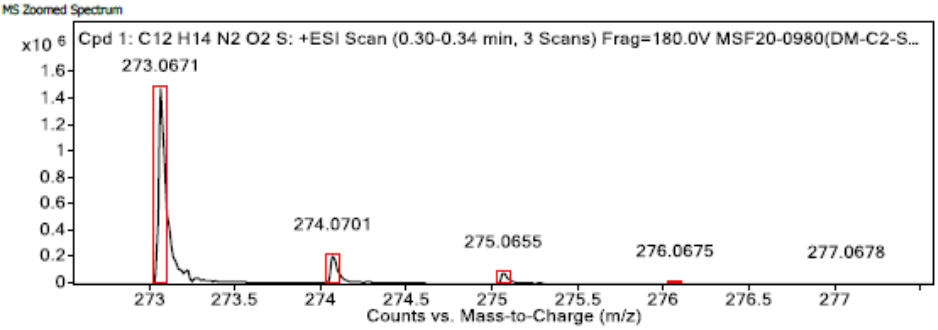

MS Spectrum Peak List

Obs. m/z	Calc. m/z	Charge	Abundance	Formula	Ion Species	Tgt Mass Error (ppm)
273.0671	273.0668	1	1484285	C12H14N2O2S	(M+Na)+	-1.13
274.0701	274.0697	1	212413	C12H14N2O2S	(M+Na)+	-1.47
275.0655	275.0649	1	80741	C12H14N2O2S	(M+Na)+	-2.13
276.0675	276.0669	1	9673	C12H14N2O2S	(M+Na)+	-2.08
277.0678	277.0679	1	1457	C12H14N2O2S	(M+Na)+	0.65

--- End Of Report ---

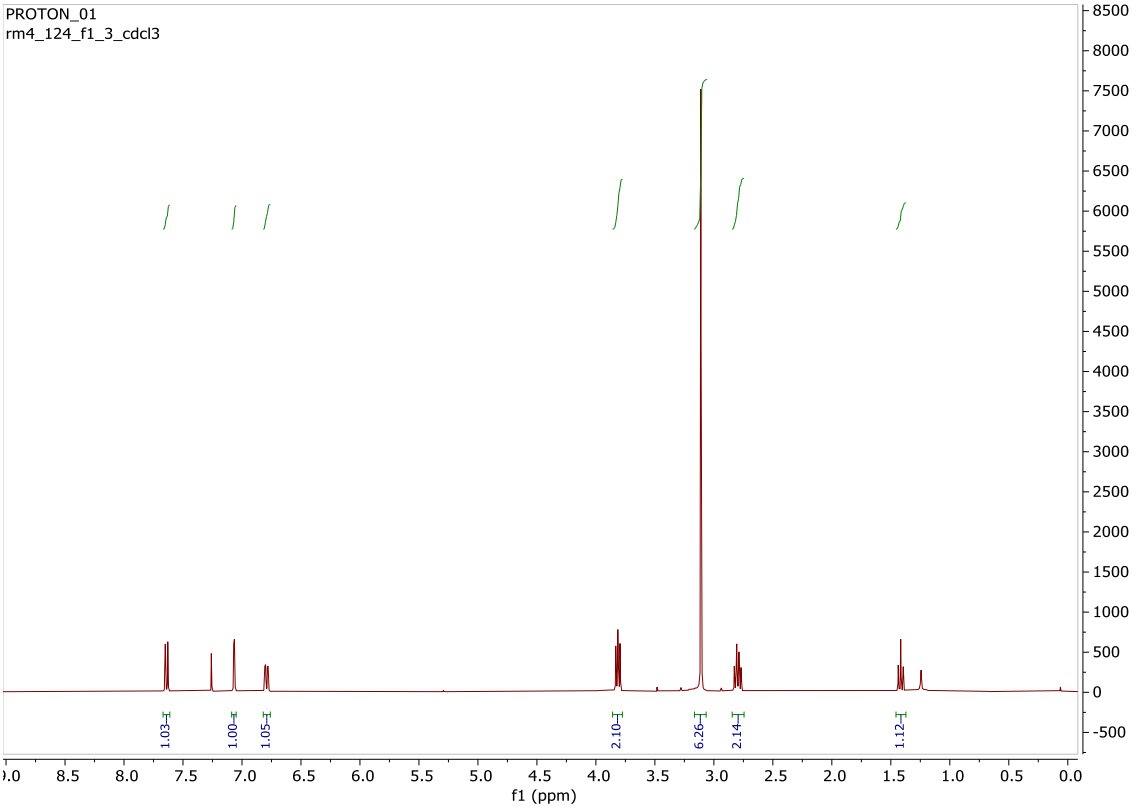

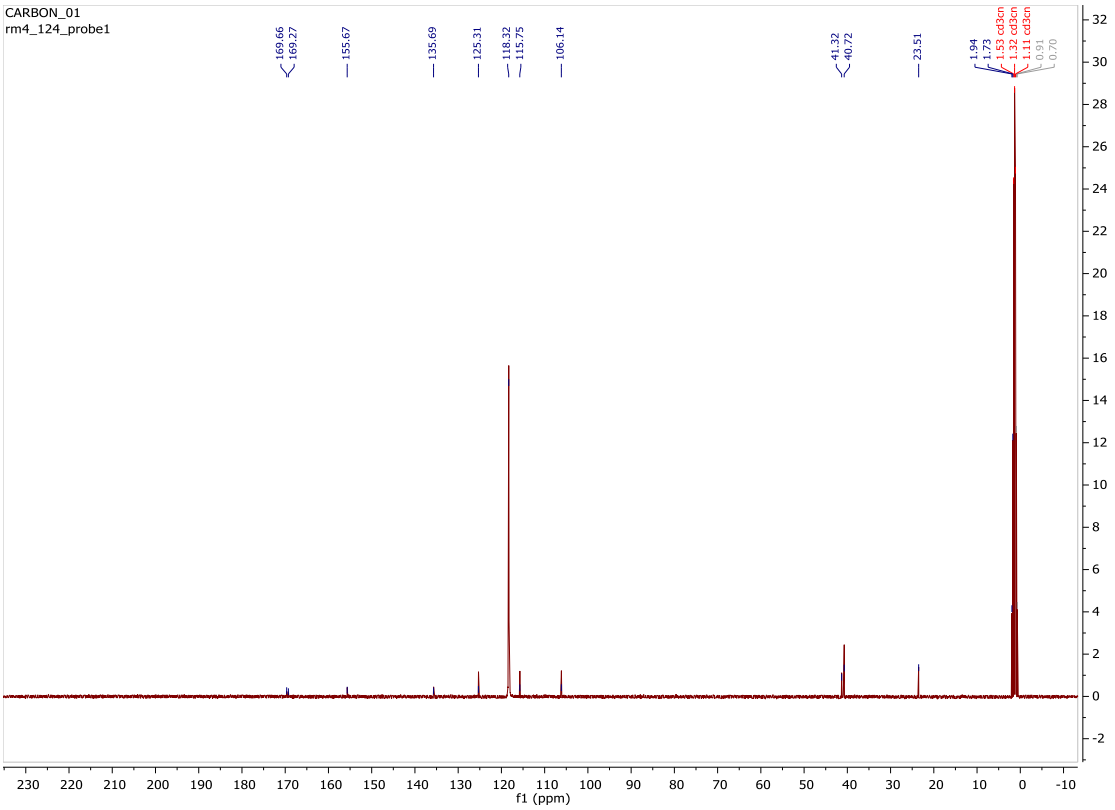

Probe **2**

Target Compound Screening Report

Results Acquired by The University of Texas at Austin Mass Spectrometry Facility

Data File	MSF20-0252(DM-Gly)_hrESIpos4.d	**Sample Name**	0252(DM-Gly)	**Comment**	0252(DM-Gly)
Position	P1-C6	**Instrument Name**	Instrument 1	**User Name**	
Acq Method	FIA_pos.m	**Acquired Time**	2/25/2020 1:19:47 PM	**DA Method**	KS.m

MS Zoomed Spectrum

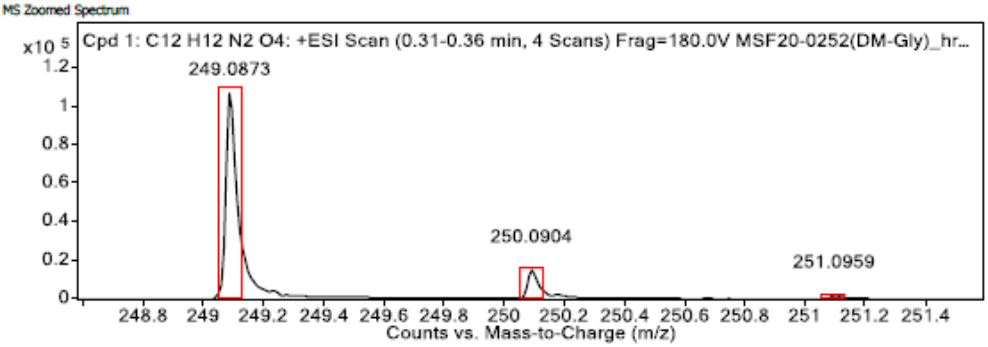

MS Spectrum Peak List

Obs. m/z	Calc. m/z	Charge	Abundance	Formula	Ion Species	Tgt Mass Error (ppm)
249.0873	249.0870	1	108818	C12H12N2O4	(M+H)+	-1.15
250.0904	250.0900	1	15347	C12H12N2O4	(M+H)+	-1.52
251.0959	251.0922	1	2145	C12H12N2O4	(M+H)+	-14.71
252.0867	252.0947	1	295	C12H12N2O4	(M+H)+	31.64
271.0698			358290			

--- End Of Report ---

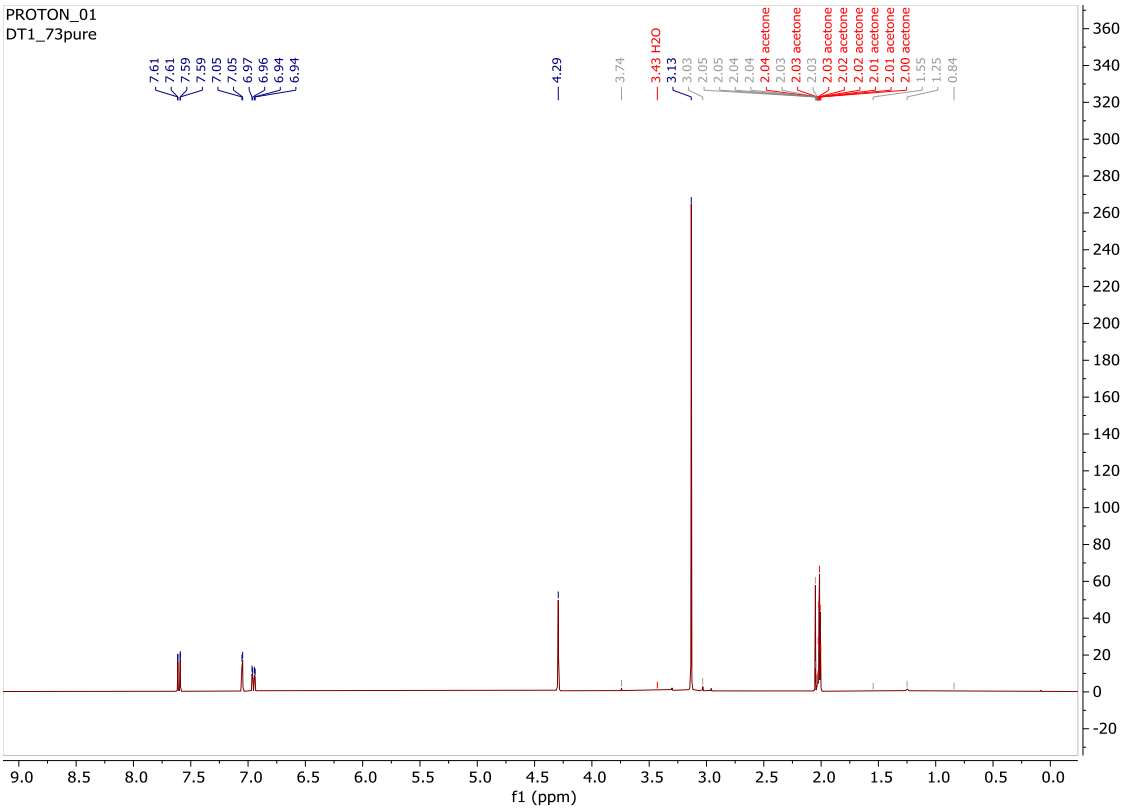
PROTON_01
DT1_73pure
7.61
7.61
7.59
7.59
7.05
7.05
6.97
6.96
6.94
6.94
4.29
3.74
3.43 H2O
3.13
3.03
2.05
2.04
2.04 acetone
2.03
2.03 acetone
2.03
2.03 acetone
2.02 acetone
2.02 acetone
2.01 acetone
2.01 acetone
2.00 acetone
1.55
1.25
0.84
f1 (ppm)

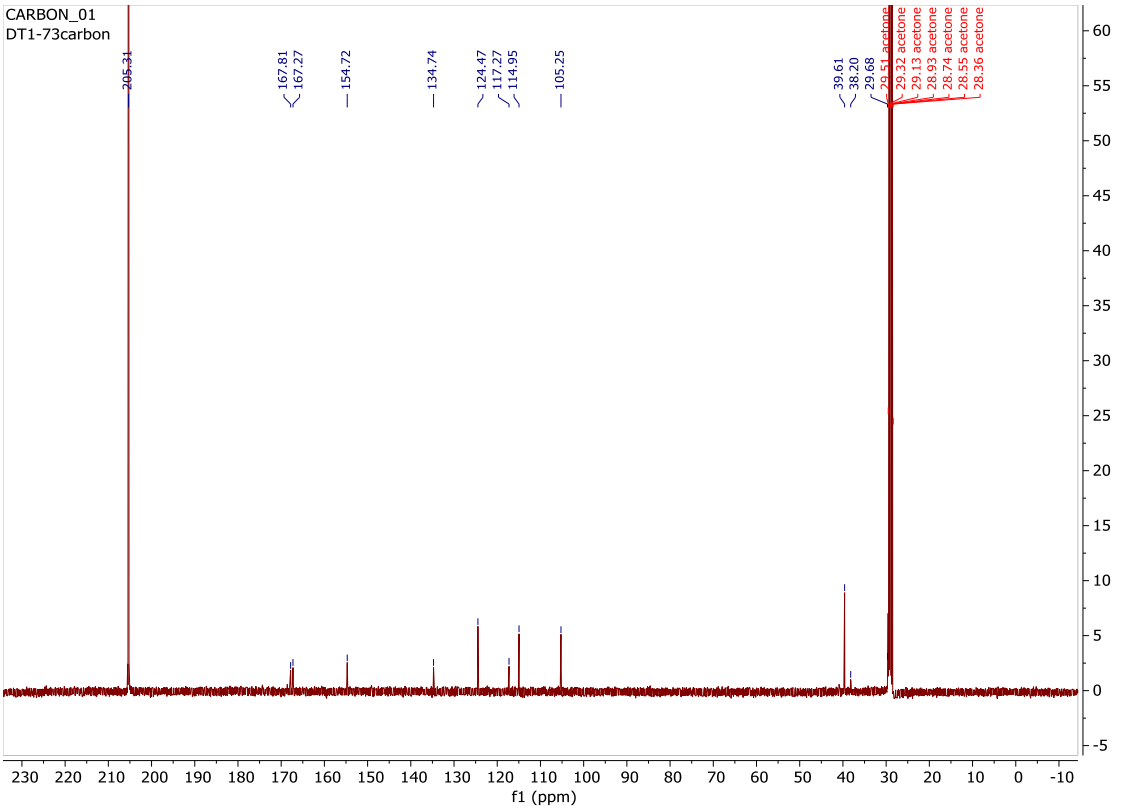
CARBON_01
DT1-73carbon
206.31
167.81
167.27
154.72
134.74
124.47
117.27
114.95
105.25
39.61
38.20
29.68
29.51 acetone
29.32 acetone
29.13 acetone
28.93 acetone
28.74 acetone
28.55 acetone
28.36 acetone
f1 (ppm)

Probe **3D**

Target Compound Screening Report

Results Acquired by The University of Texas at Austin Mass Spectrometry Facility

Data File	MSF19-1177(DM-D-Cys)_hrESIpos2.d	**Sample Name**	1177(DM-D-Cys)	**Comment**	1177(DM-D-Cys)
Position	P1-F7	**Instrument Name**	Instrument 1	**User Name**	
Acq Method	pos.m	**Acquired Time**	6/25/2019 10:35:23 AM	**DA Method**	KS.m

MS Zoomed Spectrum

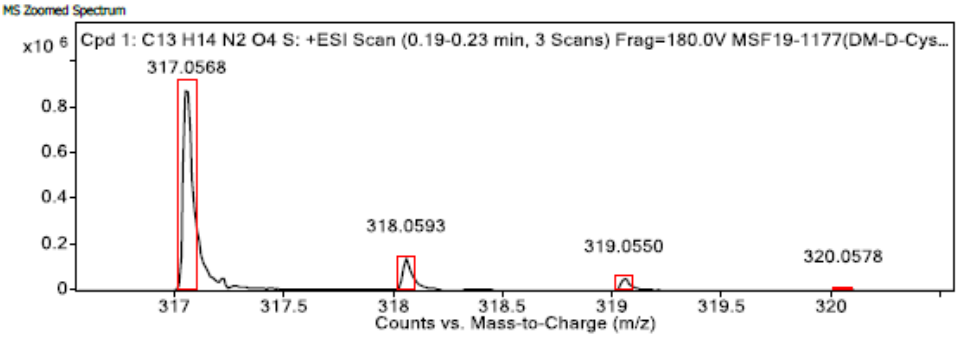

MS Spectrum Peak List

Obs. m/z	Calc. m/z	Charge	Abundance	Formula	Ion Species	Tgt Mass Error (ppm)
317.0568	317.0566	1	912298	C13H14N2O4S	(M+Na)+	-0.56
318.0593	318.0596	1	140779	C13H14N2O4S	(M+Na)+	0.7
319.0550	319.0553	1	51814	C13H14N2O4S	(M+Na)+	1.04
320.0578	320.0574	1	7250	C13H14N2O4S	(M+Na)+	-1.12
321.0609	321.0583	1	1502	C13H14N2O4S	(M+Na)+	-8.12

--- End Of Report ---

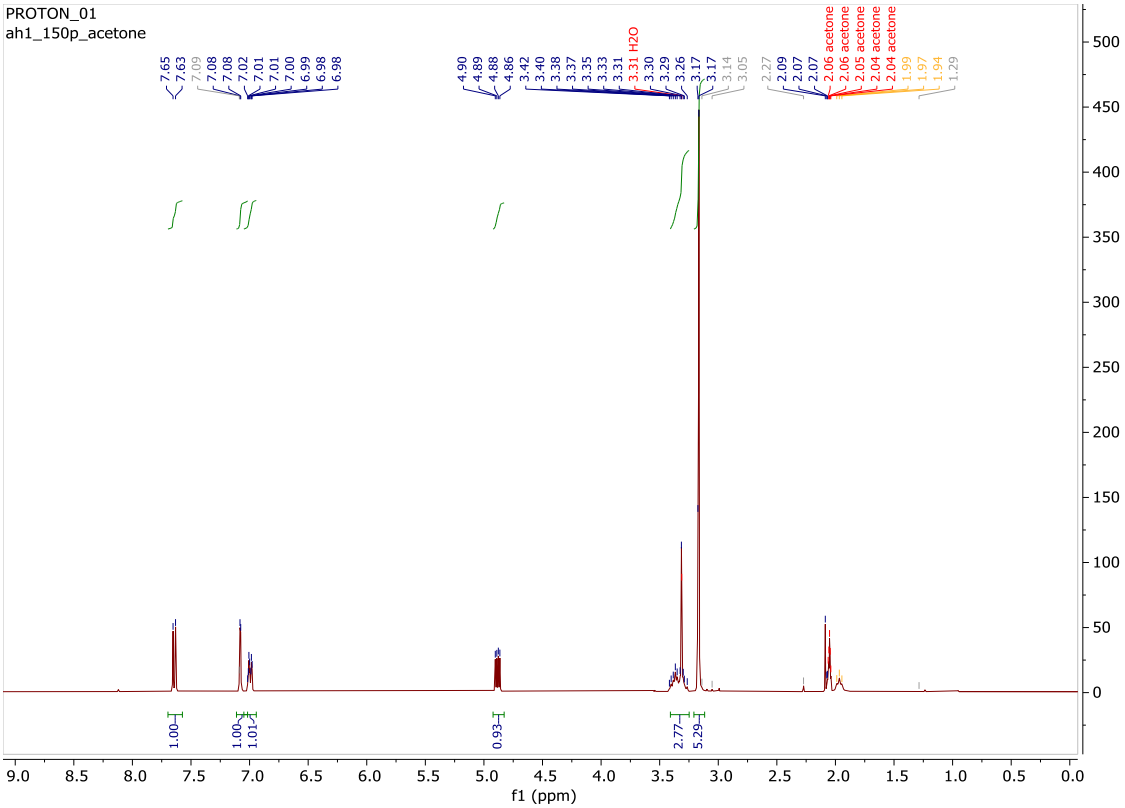

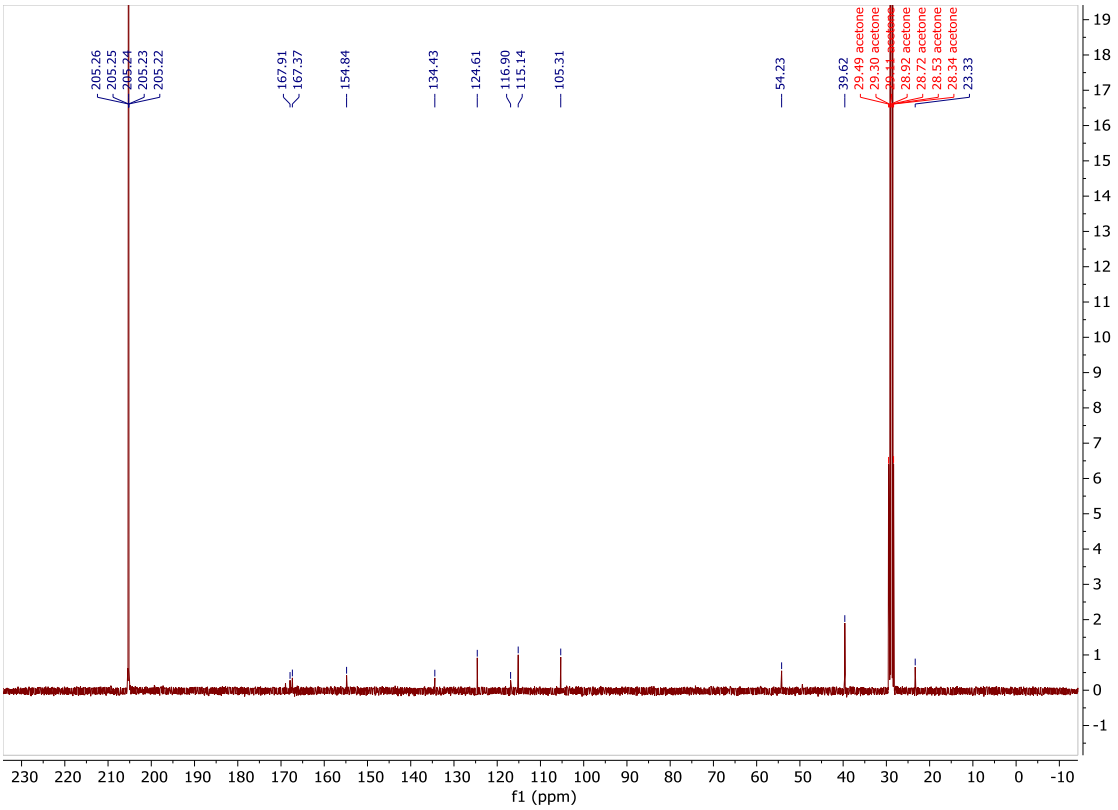

Probe **4D**

Target Compound Screening Report

Results Acquired by The University of Texas at Austin Mass Spectrometry Facility

Data File	MSF19-1826(DM-D-CYS-ESTER-4D)_hrESIpos1.d	**Sample Name**	1826(DM-D-CYS-ESTER-4D)	**Comment**	1826(DM-D-CYS-ESTER-4D)
Position	P1-F5	**Instrument Name**	Instrument 1	**User Name**	
Acq Method	FIA_pos.m	**Acquired Time**	10/14/2019 8:53:12 AM	**DA Method**	KS.m

MS Zoomed Spectrum

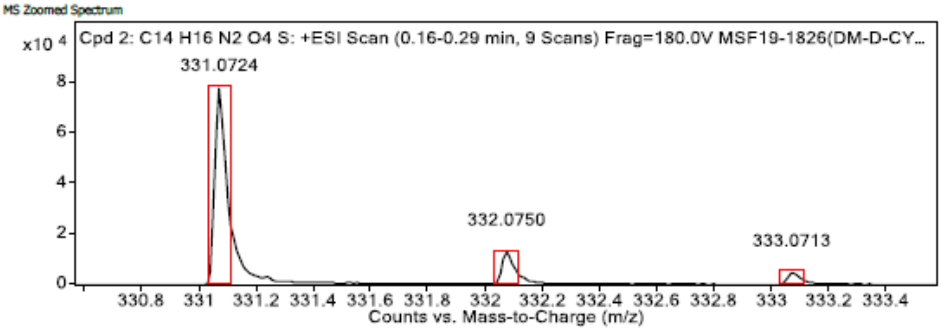

MS Spectrum Peak List

Obs. m/z	Calc. m/z	Charge	Abundance	Formula	Ion Species	Tgt Mass Error (ppm)
331.0724	331.0723	1	77969	C14H16N2O4S	(M+Na)+	-0.28
332.0750	332.0752	1	13154	C14H16N2O4S	(M+Na)+	0.84
333.0713	333.0712	1	4893	C14H16N2O4S	(M+Na)+	-0.36
334.0751	334.0732	1	719	C14H16N2O4S	(M+Na)+	-5.84
335.0749	335.0742	1	144	C14H16N2O4S	(M+Na)+	-2.09

--- End Of Report ---

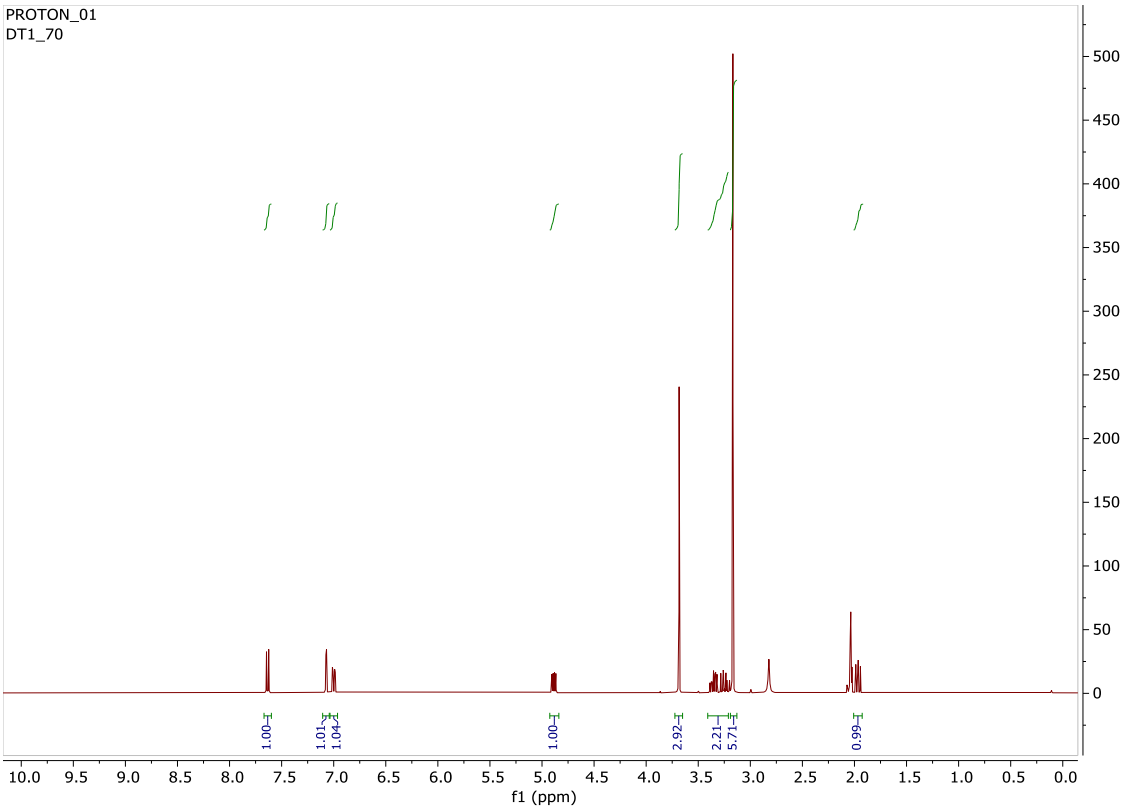
PROTON_01
DT1_70
1.00
1.01
1.04
1.00
2.92
2.21
5.71
0.99
f1 (ppm)

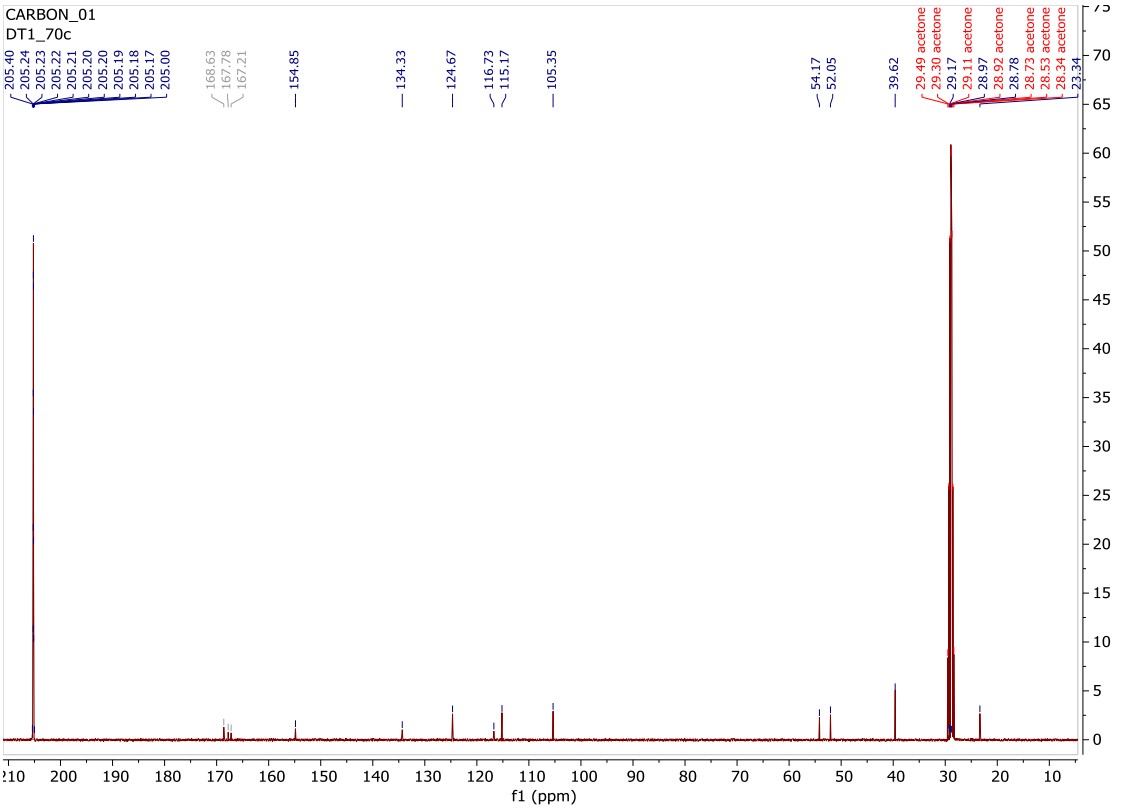
CARBON_01
DT1_70c
205.40
205.24
205.23
205.22
205.21
205.20
205.20
205.19
205.18
205.17
205.00
168.63
167.78
167.21
154.85
134.33
124.67
116.73
115.17
105.35
54.17
52.05
39.62
29.49 acetone
29.30 acetone
29.17
29.11 acetone
28.97
28.92 acetone
28.78
28.73 acetone
28.53 acetone
28.34 acetone
23.34
f1 (ppm)

Probe **3L**

Target Compound Screening Report

Results Acquired by The University of Texas at Austin Mass Spectrometry Facility

Data File	MSF20-0981(DM-L-Cys (3L))_hrESIpos1.d	**Sample Name**	0981(DM-L-Cys (3L))	**Comment**	0981(DM-L-Cys (3L))
Position	P1-A2	**Instrument Name**	Instrument 1	**User Name**	
Acq Method	FIA_pos.m	**Acquired Time**	9/25/2020 10:38:13 AM	**DA Method**	KS.m

MS Zoomed Spectrum

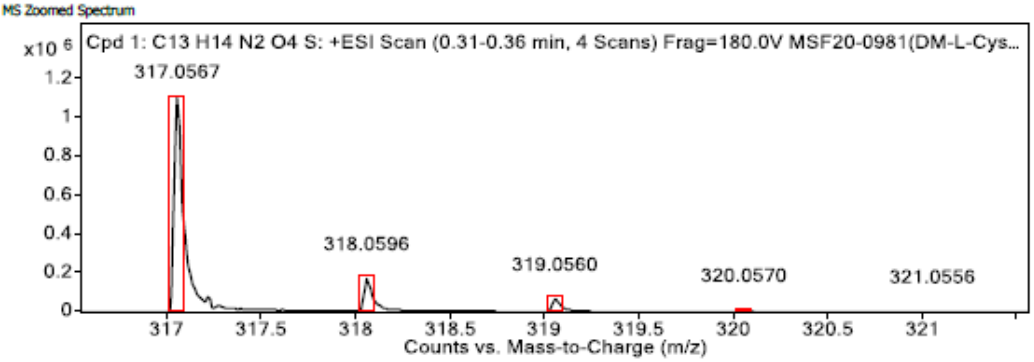

MS Spectrum Peak List

Obs. m/z	Calc. m/z	Charge	Abundance	Formula	Ion Species	Tgt Mass Error (ppm)
317.0567	317.0566	1	1109630	C13H14N2O4S	(M+Na)+	-0.24
318.0596	318.0596	1	171758	C13H14N2O4S	(M+Na)+	-0.23
319.0560	319.0553	1	65220	C13H14N2O4S	(M+Na)+	-2.22
320.0570	320.0574	1	8651	C13H14N2O4S	(M+Na)+	1.2
321.0556	321.0583	1	1348	C13H14N2O4S	(M+Na)+	8.56

--- End Of Report ---

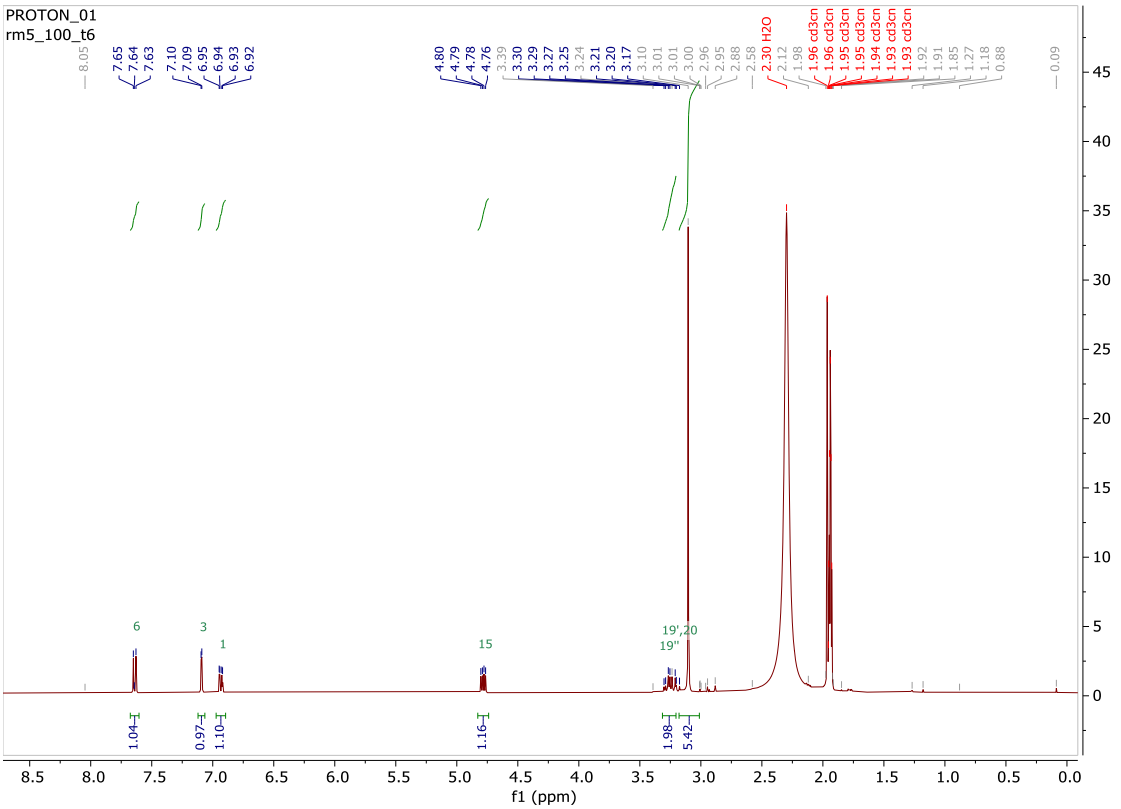

Probe **4L**

Target Compound Screening Report

Results Acquired by The University of Texas at Austin Mass Spectrometry Facility

Data File	MSF20-0982(DM-L-Cys ESTER(4L))_hrESIpos1.d	**Sample Name**	0982(DM-L-Cys ESTER(4L))	**Comment**	0982(DM-L-Cys ESTER(4L))
Position	P1-A3	**Instrument Name**	Instrument 1	**User Name**	
Acq Method	FIA_pos.m	**Acquired Time**	9/25/2020 10:39:56 AM	**DA Method**	KS.m

MS Zoomed Spectrum

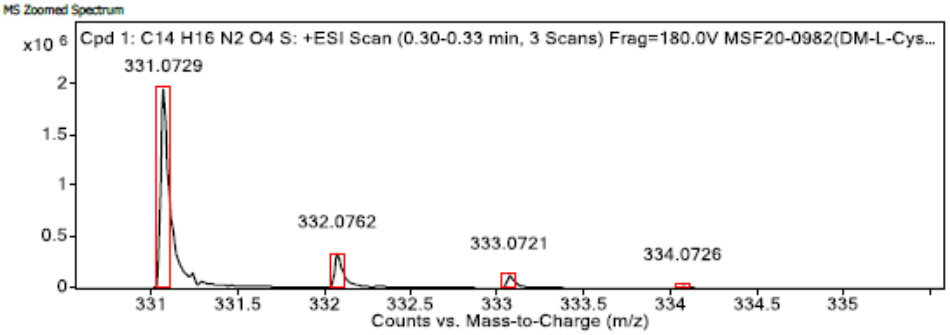

MS Spectrum Peak List

Obs. m/z	Calc. m/z	Charge	Abundance	Formula	Ion Species	Tgt Mass Error (ppm)
331.0729	331.0723	1	1958091	C14H16N2O4S	(M+Na)+	-1.94
332.0762	332.0752	1	336197	C14H16N2O4S	(M+Na)+	-2.82
333.0721	333.0712	1	124497	C14H16N2O4S	(M+Na)+	-2.64
334.0726	334.0732	1	16426	C14H16N2O4S	(M+Na)+	1.59

--- End Of Report ---

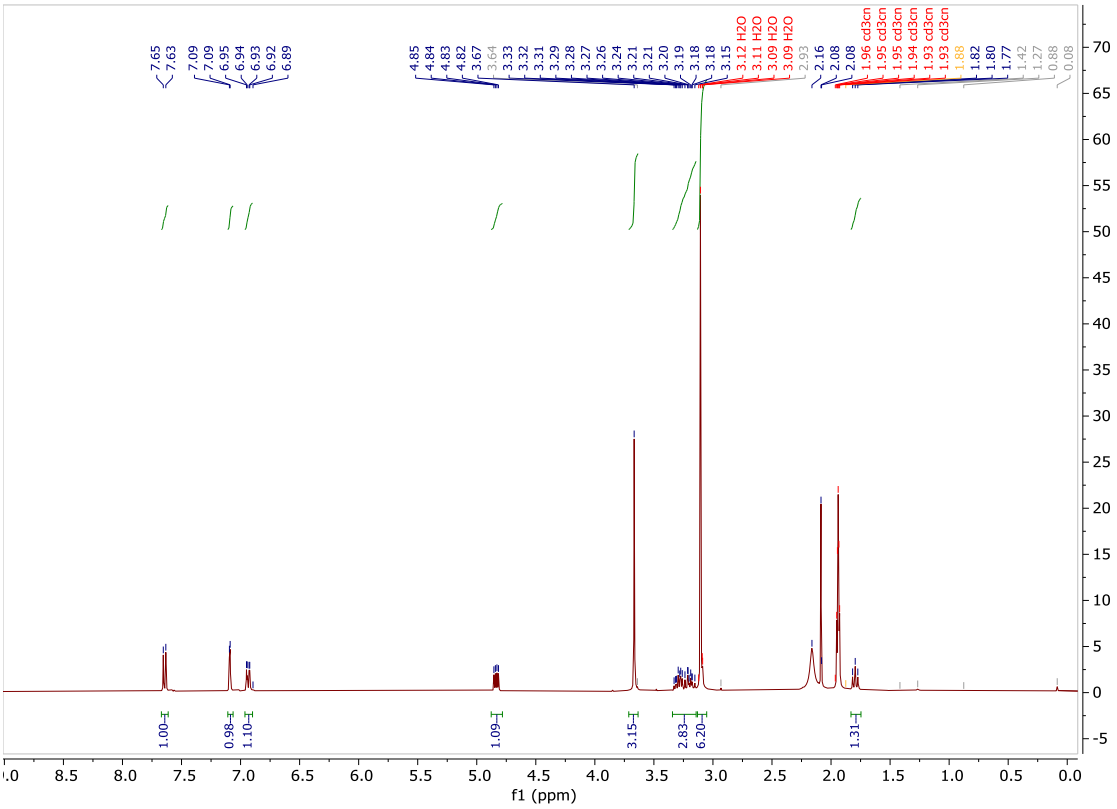

Probe **4D-SMe**

Target Compound Screening Report

Results Acquired by The University of Texas at Austin Mass Spectrometry Facility

Data File	MSF21-0496(4D-SMe)_hrESIpos7.d	**Sample Name**	0496(4D-SMe)	**Comment**	0496(4D-SMe)
Position	P1-F1	**Instrument Name**	Instrument 1	**User Name**	
Acq Method	FIA_pos.m	**Acquired Time**	3/29/2021 4:13:24 PM	**DA Method**	KS.m

MS Zoomed Spectrum

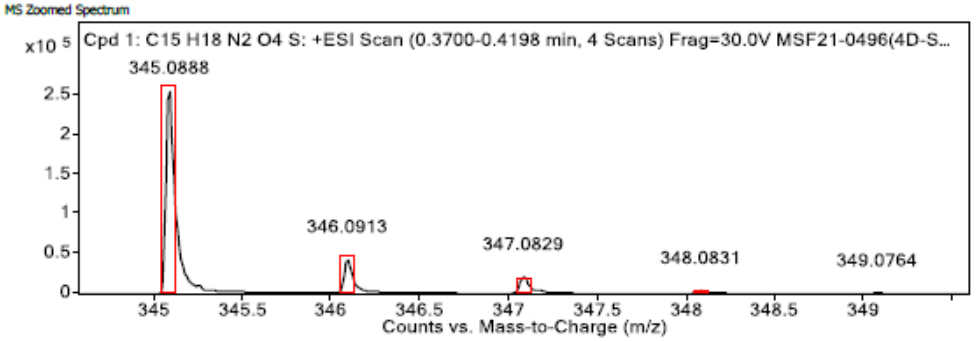

MS Spectrum Peak List

Obs. m/z	Calc. m/z	Charge	Abundance	Formula	Ion Species	Tgt Mass Error (ppm)
345.0888	345.0879	1	258683	C15H18N2O4S	(M+Na)+	-2.56
346.0913	346.0909	1	43398	C15H18N2O4S	(M+Na)+	-1.21
347.0829	347.0870	1	21397	C15H18N2O4S	(M+Na)+	11.96
348.0831	348.0889	1	3938	C15H18N2O4S	(M+Na)+	16.61
349.0764	349.0900	1	761	C15H18N2O4S	(M+Na)+	38.87
350.0716	350.0918	1	451	C15H18N2O4S	(M+Na)+	57.73
598.0808			259328			

--- End Of Report ---